Lumbar Spine Mechanical Response to Combined Flexion and Compression in Post-Mortem Human Subjects

Michael R. Burns, A. James Caldwell, Sara H. Sochor, Jeesoo Shin,
Connor J. Hanggi, Bronislaw Gepner, Jason R. Kerrigan

Abstract The goal of this study was to evaluate the effect of axial compression, applied by a follower load mechanism, on the response of the lumbar spine in flexion bending at flexion angles approaching failure. It characterised lumbar spine flexion and compression-displacement response while exploring sex differences and specimen degradation during testing. Seven adult lumbar post-mortem human subject (PMHS) spines (T12-S1) were tested in flexion bending with and without superimposed axial compression. Tests were performed by a 6-DOF robotic test system using a sequential loading matrix up to the point of failure. Load-deformation response data were used to characterise the kinetic response of the lumbar spine in flexion and compression. Individual vertebral kinematics were documented using 3D motion capture for bending deformation and specimen change analysis. This study found: (1) the response in kinetics and kinematics of the PMHS lumbar spine changes due to repeated loading; (2) total spine flexion angle is unevenly distributed across individual joints; (3) the kinetic response is stiffer with compression at low angles, but the stiffness is similar with and without axial compression approaching the failure threshold.

Keywords Compression, Flexion, Follower load, Lumbar spine, PMHS.

I. INTRODUCTION

The introduction of autonomous driving systems (ADS) has resulted in automotive industry interest in the use of non-standard vehicle seating positions, breaking from the historic limitations to seatback recline angles during driving [1-3]. Anticipation of novel seating postures in autonomous vehicles has led to substantial research on the injuries to occupants with reclined seatbacks positioned away from an instrument panel and knee bolster [2-4]. Such arrangement may require occupants to be restrained by only the seatbelt and seat. In frontal crashes with reclined occupants and strong pelvis restraint, human body model (HBM) simulations have suggested the lumbar spine would be subjected to simultaneously high compression and flexion loading [5-9]. In these simulations, the reclined orientation of the torso and the pelvic restraint offered by the seat and lap belt initially result in lumbar compression. If a shoulder-belt force limiter is engaged, the upper torso may then translate forward, potentially bringing the head and upper torso forward of the pelvis. Such torso kinematics result in lumbar spine flexion, which becomes superimposed on the compression present from earlier motion. This compression/flexion loading mechanism in frontal crashes with reclined occupants has also been illustrated in sled tests with post-mortem human subjects (PMHS) that sustained lumbar spine fractures characteristic of compression/flexion loading and with anthropomorphic test devices (ATDs) that measured high magnitude compression and flexion loads [10-12].

Previous studies showed the mechanical response or “stiffness” of lumbar spine functional spinal units (FSUs) (two vertebrae) in bending, and shear is affected by superposition of axial compressive loads [13-17]. While these data provide kinetic (force and moment) response information for FSUs, they lack a description of how spinal flexion kinematics (translation and rotation) are distributed across the individual vertebral motion segments of the lumbar spine. While such information could be obtained from experiments in which the whole lumbar spine (more than two-vertebrae FSUs) is subjected to combined compression and flexion, the lumbar spine has been shown to be unstable and eventually buckle under compressive loads (~88 N, [18]) far lower than those experienced physiologically (600–1000 N, [19]) due to its lordotic curvature. To address this problem, Patwardhan *et al.* [20] first introduced the “follower load” loading mechanism to direct the compressive force along a path

[M]. R. Burns (e-mail: michael.r.burns@virginia.edu; tel: +1-434-297-8015) is a PhD student in Mechanical Engineering at the Center for Applied Biomechanics at the University of Virginia, USA. A. J. Caldwell is a Research Engineer, S. H. Sochor is the Anatomical Donations Coordinator, J. Shin is a Research Engineer, B. Gepner is a Senior Scientist, C. J. Hanggi is a MS student, and J. R. Kerrigan is an Associate Professor at the Center for Applied Biomechanics in the Department of Mechanical Engineering at the University of Virginia, USA.

that approximates the tangent of the spine's curvature, which substantially increased the compressive load-carrying capacity of the spine without buckling. This was accomplished by attaching cable guides bilaterally to the L2 through L5 vertebral bodies with the L1 body potted, then feeding steel cables through the cable guides and attaching an anchor weight sufficient to impose 1200 N of compressive follower load. While several additional studies have employed the use of a follower load mechanism to evaluate lumbar spine response to the effect of axial compression, these studies have used low magnitude loading to investigate sources for lower-back pain [21-28].

Response data for the human lumbar spine are needed to evaluate the biofidelity of ATDs and HBMs. Our previous study used a follower-load mechanism to investigate the response of the lumbar spine with loading magnitudes relevant for occupant crash/traumatic injury situations at non-injurious, low flexion/extension and lateral bending angles [29-30]. The aim of this study was to evaluate the effect of axial compression, applied by a follower load mechanism, on the kinetic and kinematic response of the lumbar spine in flexion bending at flexion angles that approached the failure tolerance. Flexion and compression-displacement response were observed while exploring sex differences and specimen degradation during testing.

II. METHODS

Specimen Preparation

Seven fresh-frozen, previously untested PMHS whole lumbar spine specimens (T10-coccyx) (Table AI) were obtained, stored, prepared, and tested in accordance with the ethical guidelines established by the Human Usage Review Panel of the National Highway Traffic Safety Administration (NHTSA). Additionally, all procedures were reviewed and approved by the University of Virginia Institutional Review Board-Human Surrogate Use Committee. Specimens were selected based on anthropometry and condition of the lumbar spine tissues. Specimens were stored at -18 deg. C until they were thawed for preparation during the week of testing. Between preparation and testing, specimens were stored at 4 deg. C.

Specimens were carefully dissected to remove extraneous soft tissue, leaving only the intact ligamentous lumbar spine (iliolumbar ligaments were removed) from T10-sacrum. 3D-printed, carbon fiber-reinforced plastic spine collars (PLA, 55% infill, 4 external layers) were rigidly affixed to the anterior L1-L4 vertebral bodies using screws. The collars were used for 3D motion tracking of individual vertebral motion and to facilitate axial compression application through the follower load. Collars were oriented parallel to the superior endplate and centered on the vertebral body in height and left/right adjustment. L5 was instrumented with two 3D motion-tracking marker trees screwed into the antero-lateral aspects of the L5 vertebral body, avoiding anterior longitudinal ligament disruption. A pressure transducer was inserted into the nucleus pulposus of the T12-L1 and L4-L5 intervertebral discs (IVD) using a hollowed precision needle insertion method without major disruption to the surrounding tissues. The inferior and superior ends of the specimens were secured in potting cups for interface with the robotic testing system. The thoracic vertebrae and sacrum were rigidly fixed to the potting cups with screws/surgical pins to hold their positions during potting. Inferiorly, the superior endplate of S1 was oriented parallel to the potting fill line and the bulk of the bilateral sacral ala were positioned below the fill line to ensure proper grip of the sacrum while allowing unrestricted motion of the L5-S1 joint. Superiorly, the T12 inferior endplate was oriented parallel to the superior potting cup fill line and positioned to facilitate good grip of the T10-T12 construct while permitting unrestricted motion of the T12-L1 joint. A polyurethane casting resin (Smooth Cast #300, Reynolds Advanced Materials, Macungie, PA) was poured to complete the rigid connection. Specimens underwent two computed tomography (CT) scans (0.65 mm slice thickness, 0.65 mm slice interval). Scans took place before specimen preparation and after specimen instrumentation. CT scans facilitated real-time vertebral motion tracking during testing by mapping 3D motion-tracking markers on the collars to the individual vertebral coordinate systems pre-defined (using anatomical landmarks) at each level (L1-L5).

Test Setup

Lumbar spine loading in flexion was applied using a six degree-of-freedom (6-DOF) force/torque and position-controlled robotic test device (KR300 R2500 Ultra, KUKA, Augsburg, Germany) (Fig. 1). Axial compressive load was applied to the specimen with a follower-load mechanism, powered by a set of independently controlled linear actuators located atop the robotic test device (AKM42G EC, Kollmorgen Corporation, Radford, VA). Both the robot and the linear actuators were controlled simultaneously using a proprietary robotic control software designed for

biomechanical testing (simVITRO, Biorobotics Group, Cleveland Clinic, USA). Motion-capture markers were fixed to the spine collars, marker trees, and potting cups and 3D motions of the vertebrae were recorded using an optoelectronic stereo-photogrammetric system (Vicon MX, Oxford, UK).

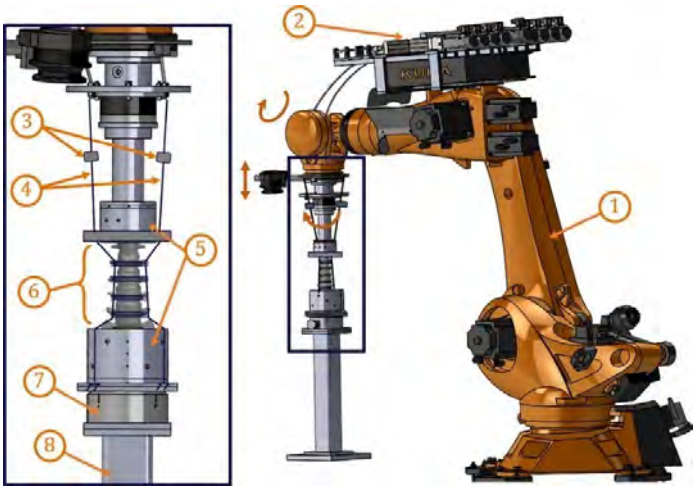

Fig. 1. Schematic showing lumbar spine specimen subjected to structural characterisation experiments: 1) the 6-DOF serial robotic test device, 2) external linear actuators, 3) follower load control load cells, 4) follower load cables, 5) specimen potting cups, 6) lumbar spine specimen, 7) robot control load cell, 8) mounting platform.

The superior and inferior potted ends of each specimen were attached to the end effector of the robot and to a 6-axis robotic control load cell mounted to a rigid pedestal, respectively (Fig. 1 and Fig. 2). To facilitate follower load application, a pair of steel cables was attached to a pair of linear actuators. The cables extended inferiorly and passed bilaterally along the specimen through cable housings on each vertebral collar, terminating at the top of the inferior potting cup. The follower load was applied through the linear actuators, which pulled the steel cables into tension with 900 N in each cable. Simultaneously, the robot's end effector applied force-controlled compression, defined normal to the superior endplate of L5, to balance the follower load while maintaining 0 N anterior-posterior (AP) shear forces.

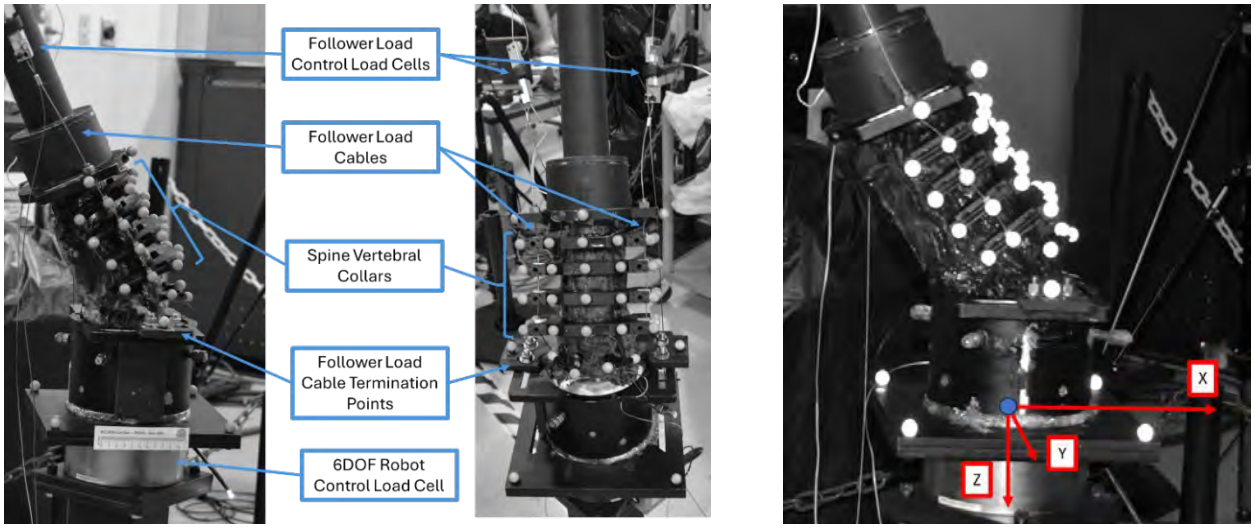

Fig. 2. Right lateral (Left) and anterior (Middle) views of an example lumbar spine specimen (sacrum inferior), in the neutral position, mounted in the robotic test fixture with the follower load cables passing bilaterally through the spine collars at L1, L2, L3, and L4. (Right) Depiction of the motion-capture coordinate frame. The origin was placed in the middle of the base plate with X pointing forward, Y pointing rightward, and Z pointing downward.

Test Methodology

A coordinate measurement machine (CMM) (ROMER Absolute Arm, Hexagon AB, Stockholm, Sweden) was used to relate the robot coordinate system to the specimen joint coordinate system (JCS), which was defined using anatomical landmark-based vertebra coordinate systems on L4 and L5 [31]. Specimen anatomical motions were defined as motions of L4 relative to L5. Translations/rotations and forces/moments were measured in the JCS. All

motion of the spine was controlled by the superior end.

To establish the neutral position of each specimen, the robot initially located the end effector (and superior potting cup) position and orientation that minimised all forces and moments in the specimen. This included the compressive force caused by gravity of the superior potting cup. The specimen was then manipulated in right and left axial rotation, right and left lateral bending, flexed, and extended until 3 Nm of corresponding resistance was established, which is called the "laxity region". The laxity region was used to establish the final neutral position as the centre of the ±3 Nm laxity region in all directions.

The optimised follower load cable position was found by adjusting the collar cable housings in the AP direction until 1800 N compressive follower load application resulted in minimised boundary flexion moment and motion capture observed individual vertebral rotations of L1-L4 of less than 4°. Determination of the neutral position and optimisation of the follower load position was done once per specimen before test matrix was performed.

Test Matrix

Flexion tests were completed via a sequential loading approach. This approach alternated between tests with and without axial compression while evaluating increasing flexion angles. A flexion angle was tested with and without compression before the next higher flexion angle was evaluated (Fig 3). Testing began at 25° without axial compression and was executed in 5° or 10° incremental increases until catastrophic failure. Catastrophic failure refers to significant and observable damage to the specimen which leaves no doubt the specimen has failed and stops additional testing. This approach allowed for evaluation of both the axially compressed and non-compressed cases at the highest possible flexion angle before specimen failure. In all tests the robotic test system applied force-controlled AP shear force minimisation and constrained all other rotations or translations to 0 deg/mm to identify motion paths that applied pure bending loading to the specimen.

During each test the spine started in the neutral position previously determined. If axial compression was applied in the test, it was first applied over a 10 second period (180 N/s) and then held for 5 s to permit equilibration. The flexion bending was applied at a constant rate (5 deg/s) to the desired angle and held for 5 seconds. Following the hold, the flexion bending was removed at the same rate as applied. There was then another 5 second hold. Finally, the axial compression was removed over a 10 second period. Specimen hydration was maintained through periodic topical saline application throughout the testing day. Tests were run approximately every 5-10 minutes throughout a single day.

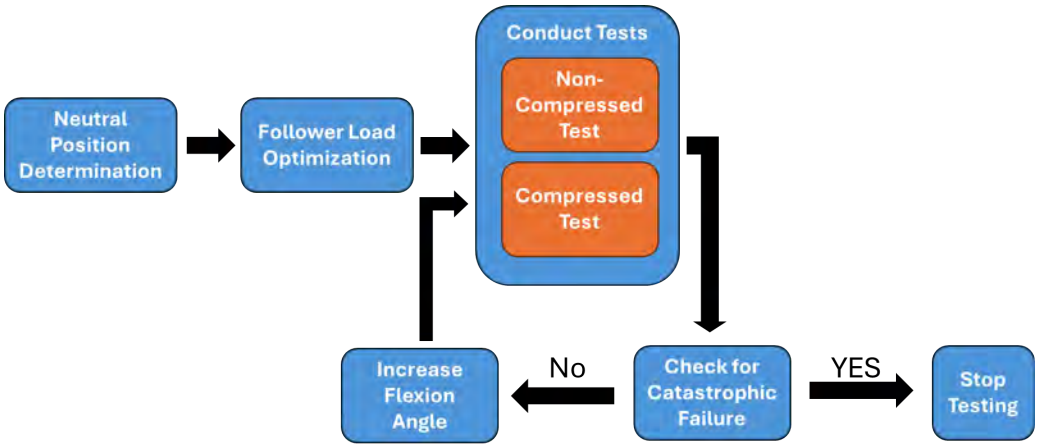

Fig. 3. Flow chart showing the decision-making process during the test matrix.

Data Processing

Total spine flexion angles and flexion moments reported are measured by the 6-DOF robot about the JCS defined above. The reported compression force is the sum of the forces measured in the two follower load control load cells. The flexion angle reported is the total flexion angle across the six free joints of the isolated lumbar spines tested (T12-S1). No filtering was used in data processing. The Wu et al [31] coordinate system definitions were used to define a vertebral coordinate system on L5. This coordinate system is projected to the end effector and when the robot moves to a new position the control system flexion is defined as the angle between the original coordinate system and the new coordinate system in the axis out of the page in the diagram (Fig. 4).

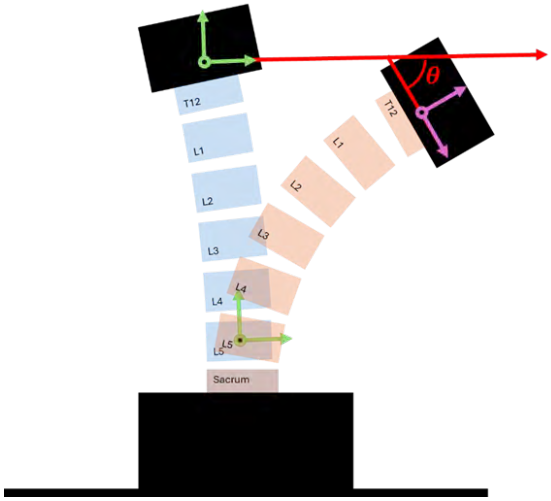

Fig 4. Depiction of the flexion definition. Blue represents t = 0, orange is at t = t. The green coordinate system was defined on L5 and projected to the top. The purple coordinate system is at time t = t. The red lines represent how the total flexion angle (θ) was determined.

Three-dimensional translations and rotations of each vertebra (L1-L5) were calculated from 3D marker motions captured by the stereo-photogrammetric system and related to the individual vertebral coordinate systems defined [31] using transformations created by identifying anatomical landmarks (and the markers themselves) from the CT data. These translations and rotations are originally reported in the motion-capture coordinate system in Fig. 2. Kinematic output flexion for an individual vertebra is defined as the rotation about the vertebra's defined y-axis. Additionally, 3D markers on the robot's end effector and the base plate were tracked to relate to the motion of T12 and the sacrum, respectively. A transformation between the end effector and T12 has not been developed; however, since they are approximately aligned during preparation and rigidly connected, they are assumed to be synonymous for these tests. A similar assumption is made between the base plate, which is tracked, and S1. These values are reported in kinematic analysis.

Displacements of the end effector (superior end) were calculated as the location of the body created using the motion-tracking markers relative to its position before any load was applied. These displacements are reported in the motion-capture coordinate frame as directional components.

The distance between adjacent vertebral bodies was calculated for each of the six free joints (e.g. L1-L2). The change in distance was measured with the motion-capture system and was defined as the distance between the calculated origin of the two bones coordinate systems. These values were normalised by the original distance between each set of vertebrae before compression was applied. Individual joint rotations were calculated from the individual vertebral coordinate systems in motion capture as the pitch of the lower body relative to the higher one's coordinate system. These values were normalised to the position before any compression was applied.

The motion-capture system periodically reported illogical or untrustworthy values due to interference. In those cases, the data were removed to prevent false data from weakening the known/accurate data, resulting in discontinuities in the data. Specimen 1042F had catastrophic damage during the setup/optimisation tests and thus had no viable response data from the sequential loading tests. It has been removed from all results, but its failure to survive the axial compression during setup is notable. Motion-capture data were not collected for specimen 945F, so it has not been included in kinematic analysis. Motion-capture data for 992M was not present for all trials and thus is reported only when available.

III. RESULTS

Sequential loading data for each specimen were evaluated to investigate the response of repeated loading, and the aggregate specimen data were evaluated to characterise the general lumbar spine flexion response. The component displacements (X, Y, Z) were examined during the compression phase of flexion tests with axial compression (Fig. 5, Appendix B). The data reported here are from the beginning of the trial through the end of compression force application. There was no flexion input during this time.

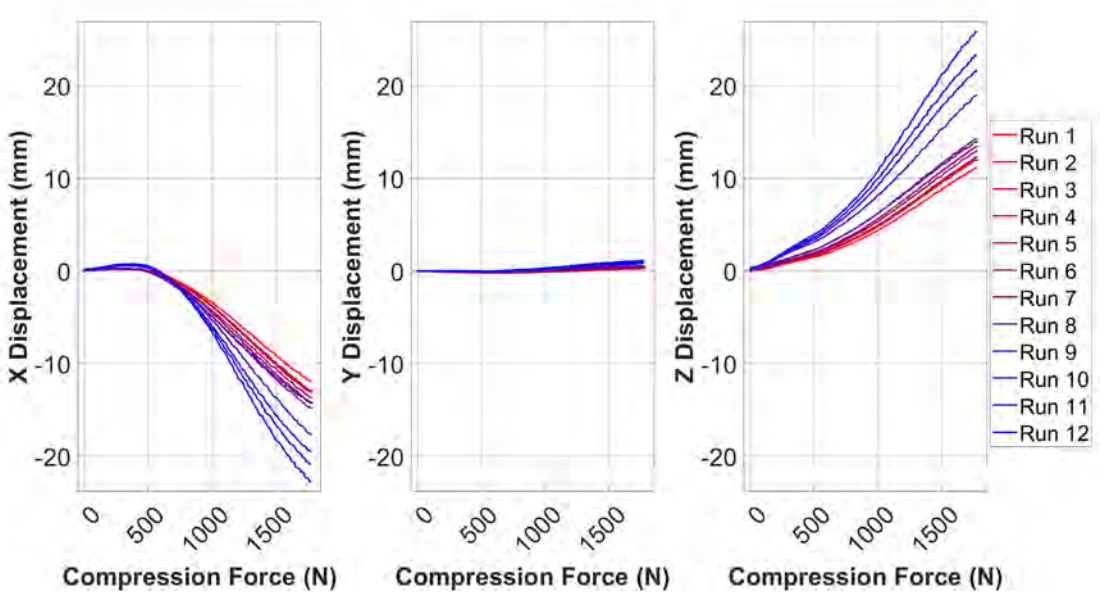

Fig. 5. Component displacements during input compression force across trials for 1007 M, other specimens are included in Appendix B. Each trial is shown with its own line. Colours progress from red to blue with each sequential test. Displacements in X are reported on the left, Y in the middle, Z on the right.

Changes in distances between the six (6) vertebral bodies in the segment were examined (Fig. 6, Appendix C). The same trials and durations of data were used as in Fig. 5.

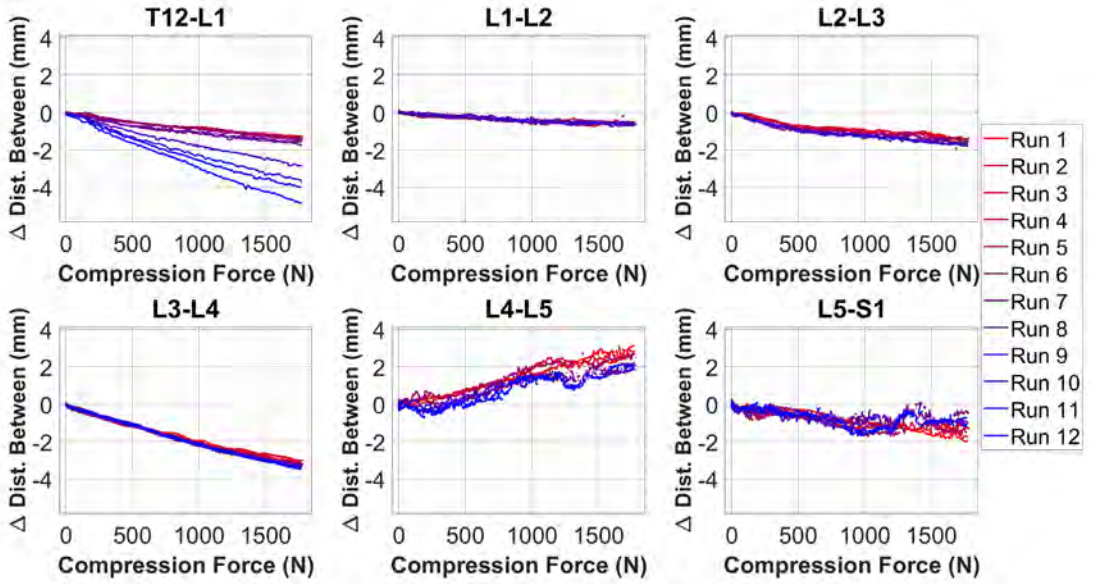

Fig. 6. Change in distance between adjacent vertebral bodies with respect to input compression force across trials for specimen 1007M; other specimens are included in Appendix C. Each trial is shown with its own line. Colours progress from red to blue with each test. Change in distance between is reported for T12-L1 (top left), L1-L2 (top middle), L2-L3 (top right), L3-L4 (bottom left), L4-L5 (bottom middle), and L5-S1 (bottom right).

The flexion moment was examined in relation to the input flexion angle during the flexing phase of tests on an individual specimen basis (Fig. 7, Appendix D). The data for the trial are plotted here from test initiation, through axial compression application, and ending once the flexion angle is fully applied. In general, we see curves shift to the right, even applying the same desired flexion angle. There is a divergence between the compressed and non-compressed tests at low angles, but that divergence diminishes at higher flexion angles.

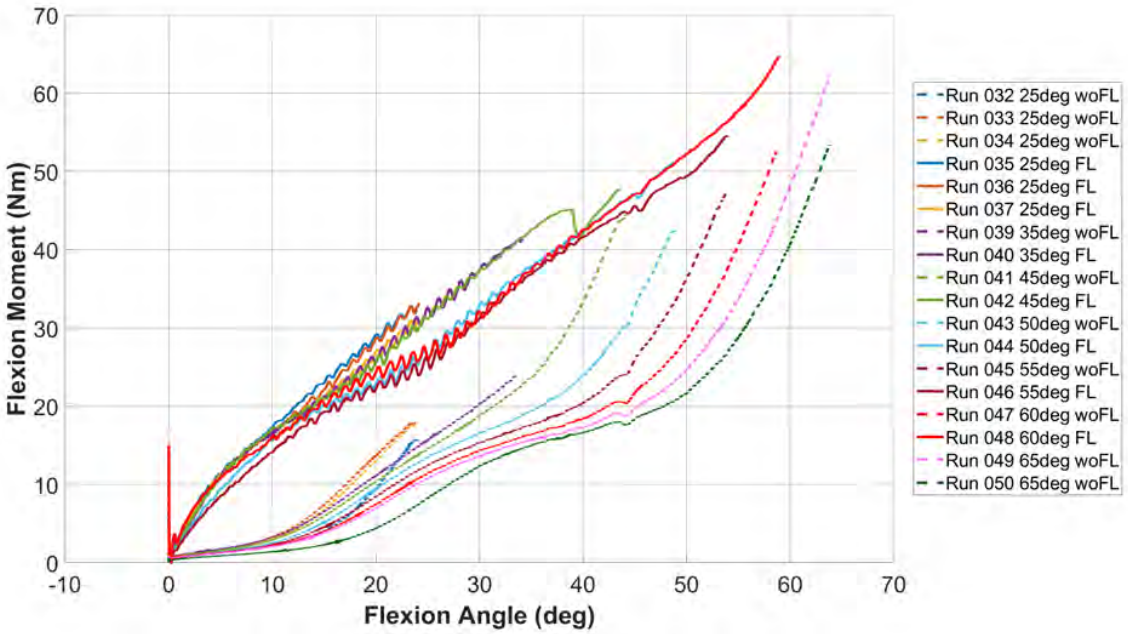

Fig. 7. Flexion moment versus flexion angle for all tests for a single specimen 1040F. Tests with and without follower load applied axial compression are included here. Each test of the sequential loading matrix is shown as its own line. Dashed lines represent the tests without axial compression, while solid lines represent the tests with axial compression. FL = test with follower load applied axial compression and woFL = test without follower load applied axial compression.

The flexion moment is reported with respect to the input flexion angle at total spine flexion angles of 25°, 35°, 45°, and 65° for tests without and with axial compression (Fig. 8). The first test in each loading condition is plotted; no repeated tests are included. The data provided here report the same duration as Fig. 7. A diminishing number of curves are provided while progressing from 25° to 65° as some of the specimens experienced catastrophic failure prior to completion of all possible tests. The data traces on these plots do not overlap consistently, but generally follow the same paths within each plot. The negative flexion moment observed at a flexion angle of zero is a result of the compression force being applied along a different line of action than where the JCS loads are measured. The flexion moments in non-compressed tests ranged from 8–23 Nm, 17–45 Nm, 25–90 Nm, and 60–145 Nm for 25°, 35°, 45°, and 65°, respectively. The flexion moments in compressed cases ranged from 8–32 Nm, 20–40 Nm, 27–56 Nm, and 50–140 Nm for 25°, 35°, 45°, and 65°, respectively.

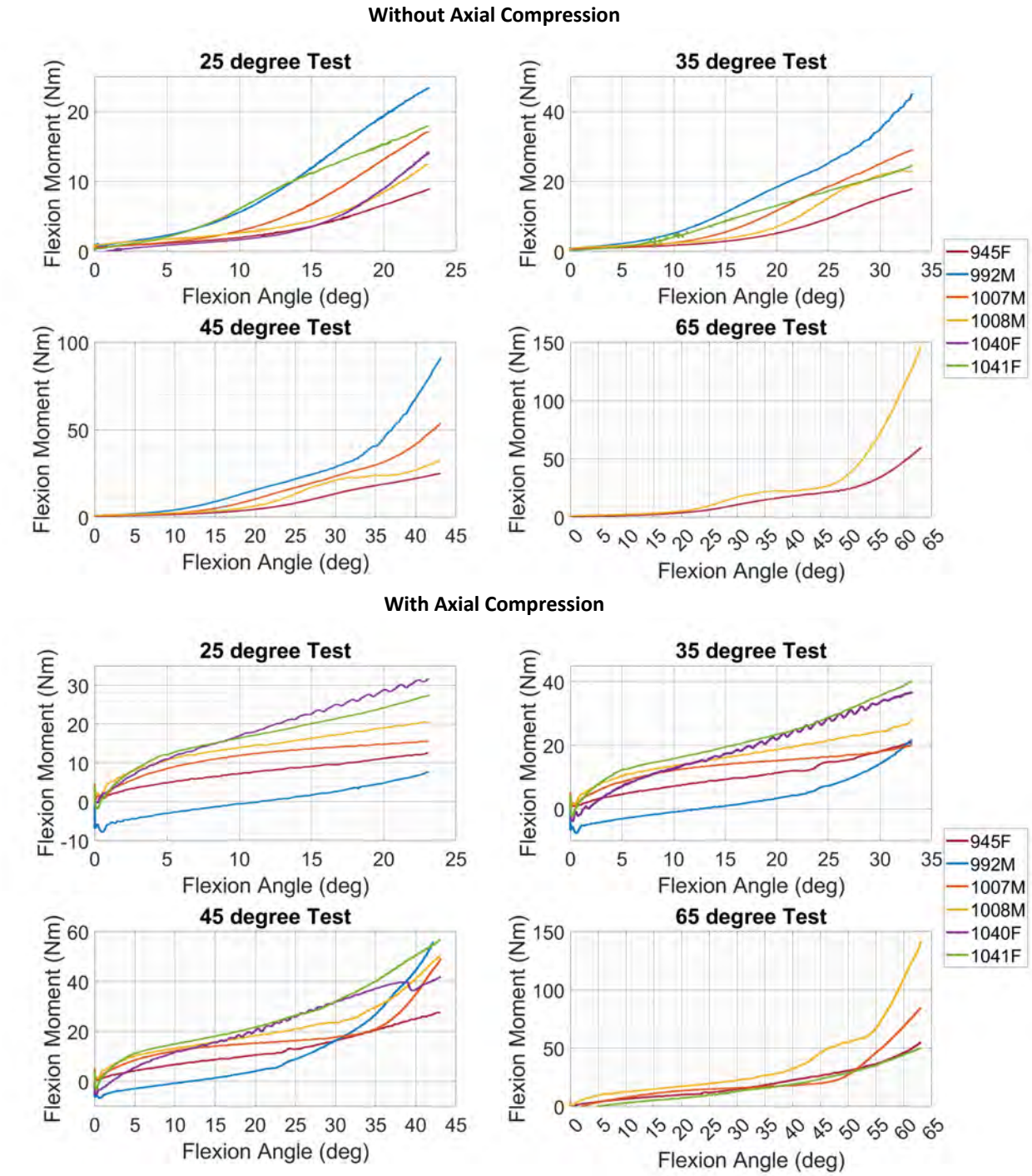

Fig. 8. Flexion moment versus flexion angle response at different flexion angle testing levels without (top) and with (bottom) axial compression. The top left shows the 25° test, top right shows the 35° test, bottom left shows the 45° test, and bottom right shows the 65° test. Each colour on these plots represents a different specimen.

The first tests from Fig. 5 are aggregated across specimens for comparison (Fig. 9). The same duration during the tests (until the end of compression) are reported as in Fig. 5 and Fig. 6. Only one test for each specimen is plotted here to report the specimens in their first tested state. The test plotted here is a 25° test with axial compression for all specimens except 992M, which plots a 35° test due to data-collection aberrations.

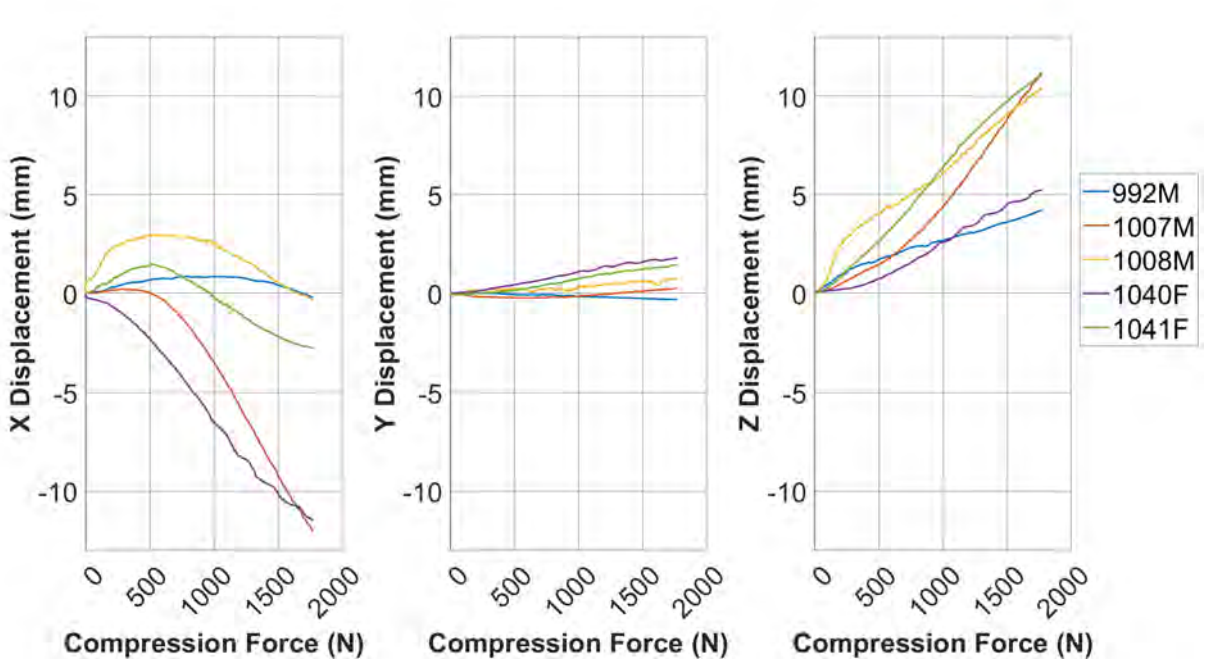

Fig. 9. Component displacements as a result of input compression force. Each line represents a different specimen from the experimental testing. X is reported on the left, Y in the middle, Z on the right.

Kinematic shape of deformation results are presented as flexion rotation contributions of each free joint with respect to the total flexion angle of the spine (Fig. 10, Appendix E). The first test in each loading condition with motion-capture data is plotted through compression application (same as Fig. 9). In some cases, non-zero local flexion angle is seen at zero total flexion angle. The angles reported represent the change in angle relative to the original angle at test initiation. On these plots we observe the same shape of the curves across different specimens.

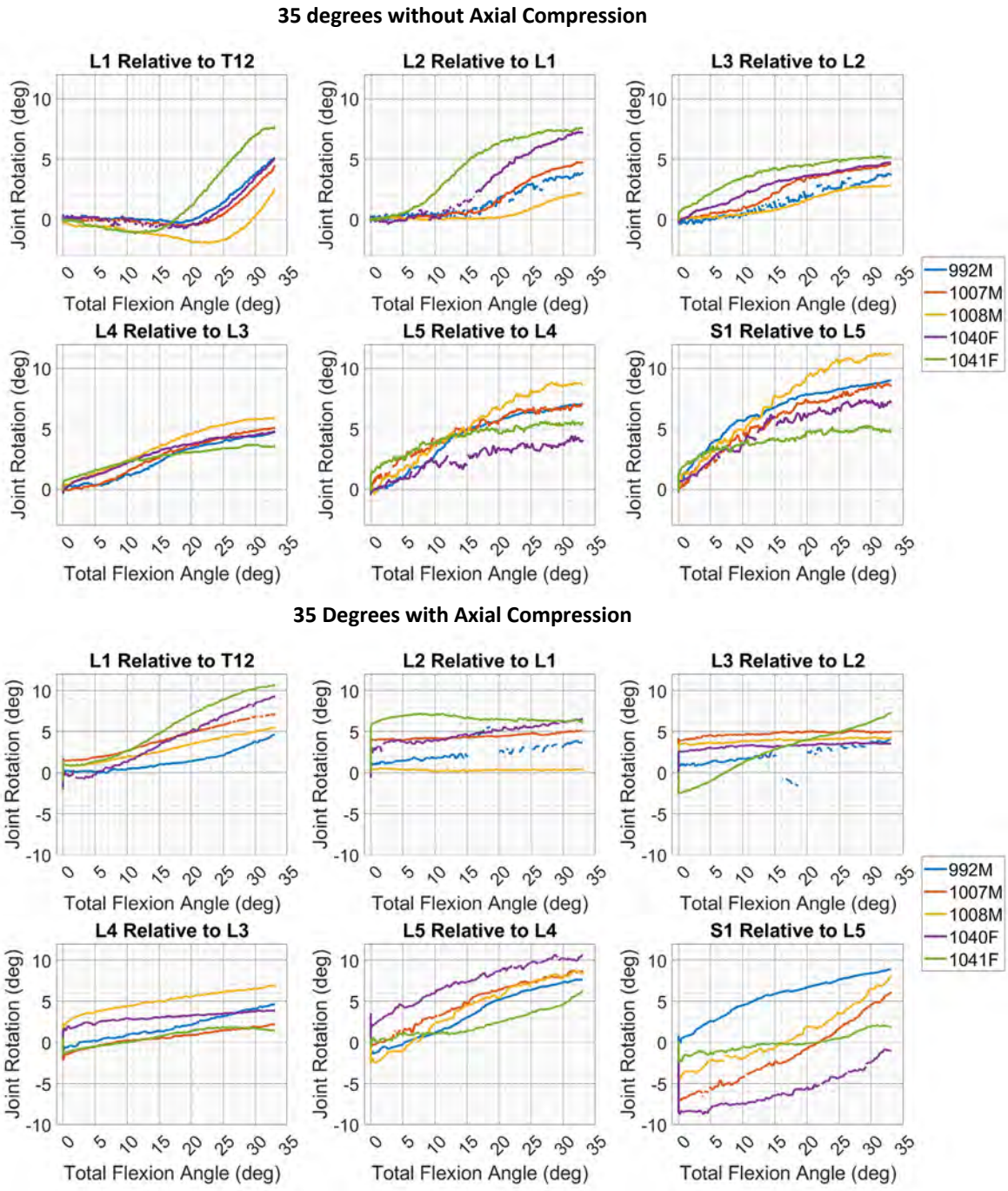

Fig. 10. Individual joint rotation for each of the six free joints versus the total spine flexion angle for 35° without axial compression (top) and with axial compression (bottom) tests. Each line represents a different specimen. The first test in each loading condition is plotted, and no repeated tests are included.

IV. DISCUSSION

The aim of this study was to characterise the response of the PMHS lumbar spine to flexion and combined compression and flexion loading at angles approaching the failure threshold. Before assessing the response, specimen viability to exhibit a consistent response under repeated loading was evaluated through the sequential loading test matrix. By observing the component displacements within a specimen relative to the initial positions during compression (1800 N), we detected changes in compressive compliance of the lumbar spine over the course of the tests (Fig. 5, Appendix B). Changes in the displacements needed to reach the compression force level were observed for all specimens, which is indicative of progressive change in specimen response over the course of testing and could be due to degradation or preconditioning. Since two vertebral bodies are separated by an IVD, a measure of the change in distance at an individual vertebral level is akin to disc height change. A certain level of disc height change during a trial would be expected during compression, but changes to these

values between sequential tests on the same specimen is indicative of changes to the properties of the spinal tissue itself or preconditioning. From the distance plots (Fig. 6, Appendix C), we observed non-uniform disc compression across vertebral levels, non-uniform progression of compression changes across IVD levels, and interspecimen variability in where compression was concentrated. The disc compression changes, especially if localised, may be a result of disc failure. This change was not localised at only the discs with the inserted pressure transducers, which suggests the sensor insertion does not cause progressive failure. The data collected by the pressure sensors are not included here, but an analysis is published separately [32].

The flexion moment versus flexion angle response for a single specimen allowed us to examine flexion bending stiffness differences (Fig. 7, Appendix D). Nonzero flexion moment was sometimes observed at zero flexion angle during compressed tests. Although follower load optimization minimized flexion rotations during compression application, if the line of action of compression was not perfectly aligned with the moment measuring location (JCS) for the vertebra a flexion moment was created at zero flexion angle because of the axial load. The observed shift to the right over consecutive tests indicates that the stiffness of the lumbar spine is decreasing between or during tests, as a greater angle is progressively required to reach the same flexion moment level. This stiffness change may be an indicator of accumulated damage or preconditioning during the sequential loading test matrix. As a result of the progressive differences observed, we realise specimens are not likely able to maintain anatomic consistency during repeated flexion and compression with flexion loading. We consider this accumulation of changed response to be progressive damage, rather than the catastrophic damage previously described. The data collected are still able to describe the response of the lumbar spine to this loading; however, the tested and changed state of the tissue must be acknowledged. As a result, future researchers should be cautioned to limit repeated loading on PMHS lumbar spines due to the changes in response observed here – we recommend that when testing the lumbar spine in future studies, the specimen only be loaded once during a single test to get the most accurate, intact response. The progressive damage along with the invasive hardware installation make it so this data should not be used for failure determination, but rather pre-failure flexion response characterization.

The biomechanical responses captured in this test series included the load-deformation (kinetic) response, measured in bending moment relative to bending angle, and the kinematic response, which describes how the deformation of the spine is distributed across the individual intervertebral motion segments throughout the spine. The flexion moment and flexion angle curve shape (Fig. 7, Appendix D) give insight into the flexion bending stiffness and differences between how the lumbar spine loads in pure flexion and flexion combined with superimposed axial compression. The divergence between compressed and non-compressed response observed in the specimen specific curves at lower angles has been previously described [29]. To our knowledge, the current study is the first evaluation of the PMHS lumbar spine response under these loading conditions, and the described convergence at higher flexion angles has not been previously discerned.

There is an observed time in all the specimens' responses where the data traces with and without compression seem to converge; however, this varies by specimen. This intersection point has not been previously explained and implies the sensitivity to the presence of axial compression diminishes at higher flexion angles. The flexion angle at which the traces converge varies across specimens and could be attributable to anatomical differences in geometry. When examining the flexion moment versus angle response for all specimens, there are no assurances all reported responses are non-disrupted due to progressive damage that is likely to have begun. Although the PMHS spine response may not be representative of a definitively healthy and untested lumbar spine, it does exemplify the characteristic behaviour noted across specimens and represents the best experimental data available to us at this time. Even with the observed and described issues, these data are likely useful for HBM lumbar spine modeling and response tuning.

In the aggregated responses, we observed similar distributions of flexion moments at the lower flexion angles as previously reported [29]. Across all angles and loading conditions, there is a similar shape of the loading curve, leading to the conclusion that we have positively identified a characteristic stiffening behaviour (Fig. 8). We observe a lack of overlap in the aggregated response, which represents inter-specimen variability. We observe bilinear behaviour with a stiffened response at higher flexion angles, likely due to the engagement of a different anatomical region or structure at higher flexion angles. The inflection points of both the axially compressed and non-compressed cases differ across specimens but are consistently present, suggesting a characteristic spine behaviour in this loading condition with specimen-specific anatomical differences causing resultant variation in the flexion angle at which structures are engaged.

Compression force and component displacement responses provide new insights into the compliance of the lumbar spine under applied axial compression. The data showed inter-specimen variability with specimens requiring a range of -12-0 mm in X displacement, 0-2 mm in Y displacement, and 4-11 mm in Z displacement to achieve 1800 N of axial compression, suggesting compliance differences across the population.

Kinematic rotation data demonstrate how individual joints contribute to the whole lumbar spine rotation (Fig. 6, Appendix C). The total flexion angle imposed on the spine is unevenly distributed across the six free joints, which could indicate a difference in stiffness by IVD level. Joints get engaged at different times for their contributions to the total flexion, as seen in the variation of when individual flexion angles change. This also differs with and without the presence of axial compression. The points at which the increase starts differs between whether axial compression is applied or not for the same driven flexion angle of the test. The total flexion angle of the test also appeared to change the joint rotation contribution, even when comparing at the same total spinal angle value (e.g. evaluating at the 25° point for a 35° and 45° test). This suggests localised joint progressive damage may be occurring. The non-zero local flexion angle observed at zero total flexion angle in some compressed cases pertains to axial compression application through the follower load. This was observed because of the inability of our methodology to remove all vertebral rotation during compression application by way of utilising the absolute vertebral pitch change. Future considerations may optimise the relative flexion angle between the vertebrae, better emphasising shape change and mitigating the initial angle during compression.

The data presented in this study provide a benchmark to assess ATDs and HBMs for the sensitivity to axial compression with flexion. Quasi-static load application was necessary in this study for the force-controlled follower load mechanism to maintain a consistent axial compression throughout the loading. This type of loading effectively illustrates the complex bending response sensitivity to axial compression dictated by the human lumbar spine anatomy. Further, both this sensitivity to axial load and the sensitivity to loading rate that is characteristic of biological tissues are biomechanical characteristics that may affect injury prediction. Thus, if ATDs and HBMs can exhibit such sensitivities, they can be deployed to better predict injury over a broad range of loading conditions. Lumbar spine loading rate-sensitivity can be measured in tissue-level experiments (e.g. tensile testing of ligaments or compression testing of IVDs) and results could be introduced into ATDs and HBMs using other methods (e.g. a scaling function to include strain-rate hardening in an HBM material or by tuning the elastomer properties in an ATD). The rate-sensitivity and the extensive hardware installation for this experimentation makes the failure tolerance of the lumbar spine more adequately captured in dynamic impact experiments with less intrusive hardware [33], where axial load sensitivity assessment was not possible because a consistent axial load could not be maintained.

This study also successfully evaluated female PMHS lumbar spines and is the first, to our knowledge, to do so in this loading scenario; however, conclusions about the sex differences in either kinetic or kinematic responses are not readily made. Previously mentioned inter-specimen variability was too high to differentiate between males and females within this limited sample size but should be a focus of future work. Future work should also investigate relationships between the specimen anatomy and its response to determine any relations.

V. CONCLUSION

In this study, flexion and flexion combined with superimposed axial compression approaching the failure threshold were performed on seven PMHS lumbar spines. Kinematic and kinetic data were collected to characterise the response of the PMHS lumbar spine in this loading mode. The following conclusions can be reached.

1. PMHS lumbar spines exhibit changes in response due to repeated flexion or flexion and compression loading.
2. PMHS lumbar spines demonstrate inter-specimen variability in kinetic and kinematic flexion responses.
3. The flexion angle applied to the lumbar spine is unevenly distributed across joint with and without compression.
4. Superposition of axial compression loading with flexion bending results in stiffer flexion response at lower angles, while the stiffnesses are similar at angles approaching the failure threshold.

VI. ACKNOWLEDGEMENTS

We would like to acknowledge the Research Consortium Concerning Automated Driving Systems (RCCADS) for their funding and contribution to this work. We would also like to acknowledge the personnel of UVA's Center for Applied Biomechanics who provided technical support for this study.

VII. REFERENCES

1. S. Koppel, J. Jiménez Octavio, K. Bohman, D. Logan, W. Raphael, L. Quintana Jimenez, & F. Lopez-Valdes, Seating configuration and position preferences in fully automated vehicles. *Traffic Injury Prevention*, **20** (2019) S103–S109. https://doi.org/10.1080/15389588.2019.1625336.
2. M. Östling & A. Larsson, *OCCUPANT ACTIVITIES AND SITTING POSITIONS IN AUTOMATED VEHICLES IN CHINA AND SWEDEN* (2019).
3. M. P. Reed, S. M. Ebert, M. L. H. Jones, & J. J. Hallman, Prevalence of non-nominal seat positions and postures among front-seat passengers. *Traffic Injury Prevention*, **21** (2020) S7–S12. https://doi.org/10.1080/15389588.2020.1793971.
4. S. Jorlöv, K. Bohman, & A. Larsson, Seating Positions and Activities in Highly Automated Cars – A Qualitative Study of Future Automated Driving Scenarios. (2017).
5. B. D. Gepner, D. Draper, K. Mroz, R. Richardson, M. Östling, B. Pipkorn, J. Forman, & J. R. Kerrigan, Comparison of Human Body Models in Frontal Crashes with Reclined Seatback. (2019).
6. B. D. Gepner, J. Toczyski, K. Rawska, D. Moreau, & J. R. Kerrigan, Sensitivity of Human Body Model Response Relative to the Lumbar Spine and Pelvic Tissue Formulation. (2020).
7. K. Rawska, B. Gepner, S. Kulkarni, K. Chastain, J. Zhu, R. Richardson, D. Perez-Rapela, J. Forman, & J. R. Kerrigan, Submarining sensitivity across varied anthropometry in an autonomous driving system environment. *Traffic Injury Prevention*, **20** (2019) S123–S127. https://doi.org/10.1080/15389588.2019.1655734.
8. K. Rawska, B. Gepner, D. Moreau, & J. R. Kerrigan, Submarining sensitivity across varied seat configurations in autonomous driving system environment. *Traffic Injury Prevention*, **21** (2020) S1–S6. https://doi.org/10.1080/15389588.2020.1791324.
9. K. Mroz, M. Östling, R. Richardson, J. Kerrigan, J. Forman, B. Gepner, N. Lubbe, & B. Pipkorn, Effect of Seat and Seat Belt characteristics on the Lumbar Spine and Pelvis Loading of the SAFER Human Body Model in reclined Postures. (2020).
10. R. Richardson, J.-P. Donlon, M. Jayathirtha, J. Forman, G. Shaw, B. Gepner, J. Kerrigan, M. Östling, K. Mroz, & B. Pipkorn, Kinematic and Injury Response of Reclined PMHS in Frontal Impacts. *Stapp car crash journal*, **64** (2020) 83–153.
11. R. Richardson, M. Jayathirtha, K. Chastain, J.-P. Donlon, J. Forman, B. Gepner, M. Östling, K. Mroz, G. Shaw, B. Pipkorn, & J. Kerrigan, Thoracolumbar spine kinematics and injuries in frontal impacts with reclined occupants. *Traffic Injury Prevention*, **21** (2020) S66–S71. https://doi.org/10.1080/15389588.2020.1837365.
12. M. Östling, C. Lundgren, N. Lubbe, A. Huf, P. Wernicke, & B. Pipkorn, The Influence of a Seat Track Load Limiter on Lumbar Spine Compression Forces in Relaxed, Reclined, and Upright Seating Positions: A Sled Test Study using THOR-50M. (2021).
13. M. Adams & P. Dolan, Time-dependent changes in the lumbar spine's resistancc to bending. *Clinical Biomechanics*, **11** (1996) 194–200. https://doi.org/10.1016/0268-0033(96)00002-2.
14. M. A. Adams & P. Dolan, Biomechanics of vertebral compression fractures and clinical application. *Archives of Orthopaedic and Trauma Surgery*, **131** (2011) 1703–1710. https://doi.org/10.1007/s00402-011-1355-9.
15. Y. Li, B. P. Kelly, & D. J. DiAngelo, Development of a Finite Element Lumbar Segment Model for Simulation of Coupled Loading Conditions Validated With In Vitro Experimental Studies. (American Society of Mechanical Engineers Digital Collection, 2013), pp. 865–866. https://doi.org/10.1115/SBC2011-53972.
16. H. S. Lin, Y. K. Liu, & K. H. Adams, Mechanical response of the lumbar intervertebral joint under physiological (complex) loading. *JBJS*, **60** (1978) 41.
17. S. W. Yang, N. A. Langrana, & C. K. Lee, BIOMECHANICS OF LUMBAR SPINE IN BIAXIAL LOADS. (1985).
18. J. J. Crisco, M. M. Panjabi, I. Yamamoto, & T. R. Oxland, Euler stability of the human ligamentous lumbar spine. Part II: Experiment. *Clinical Biomechanics*, **7** (1992) 27–32. https://doi.org/10.1016/0268-0033(92)90004-N.
19. A. L. Nachemson, Disc Pressure Measurements. *Spine*, **6** (1981) 93.
20. A. G. Patwardhan, R. M. Havey, K. P. Meade, B. Lee, & B. Dunlap, A Follower Load Increases the Load-Carrying Capacity of the Lumbar Spine in Compression. *Spine*, **24** (1999) 1003.
21. R. W. Fry, T. F. Alamin, L. I. Voronov, L. C. Fielding, A. J. Ghanayem, A. Parikh, G. Carandang, B. W. Mcintosh, R. M. Havey, & A. G. Patwardhan, Compressive Preload Reduces Segmental Flexion Instability After Progressive Destabilization of the Lumbar Spine. *Spine*, **39** (2014) E74. https://doi.org/10.1097/BRS.0000000000000093.

22. J. L. Gaffey, A. J. Ghanayem, M. L. Voronov, R. M. Havey, G. Carandang, C. Abjornson, & A. G. Patwardhan, Effect of Increasing Implant Height on Lumbar Spine Kinematics and Foraminal Size Using the ProDisc-L Prosthesis. *Spine*, **35** (2010) 1777. https://doi.org/10.1097/BRS.0b013e3181ebaa4d.
23. V. K. Goel, M. M. Panjabi, A. G. Patwardhan, A. P. Dooris, & H. Serhan, Test Protocols for Evaluation of Spinal Implants. *JBJS*, **88** (2006) 103. https://doi.org/10.2106/JBJS.E.01363.
24. P. Mageswaran, F. Techy, R. W. Colbrunn, T. F. Bonner, & R. F. McLain, Hybrid dynamic stabilization: a biomechanical assessment of adjacent and supraadjacent levels of the lumbar spine: Laboratory investigation. *Journal of Neurosurgery: Spine*, **17** (2012) 232–242. https://doi.org/10.3171/2012.6.SPINE111054.
25. A. G. Patwardhan, R. M. Havey, G. Carandang, J. Simonds, L. I. Voronov, A. J. Ghanayem, K. P. Meade, T. M. Gavin, & O. Paxinos, Effect of compressive follower preload on the flexion–extension response of the human lumbar spine. *Journal of Orthopaedic Research*, **21** (2003) 540–546. https://doi.org/10.1016/S0736-0266(02)00202-4.
26. A. Rohlmann, S. Neller, L. Claes, G. Bergmann, & H.-J. Wilke, Influence of a Follower Load on Intradiscal Pressure and Intersegmental Rotation of the Lumbar Spine. *Spine*, **26** (2001) E557.
27. S. M. Renner, R. N. Natarajan, A. G. Patwardhan, R. M. Havey, L. I. Voronov, B. Y. Guo, G. B. J. Andersson, & H. S. An, Novel model to analyze the effect of a large compressive follower pre-load on range of motions in a lumbar spine. *Journal of Biomechanics*, **40** (2007) 1326–1332. https://doi.org/10.1016/j.jbiomech.2006.05.019.
28. H.-J. Wilke, A. Rohlmann, S. Neller, F. Graichen, L. Claes, & G. Bergmann, ISSLS Prize Winner: A Novel Approach to Determine Trunk Muscle Forces During Flexion and Extension: A Comparison of Data From an: In Vitro: Experiment and: In Vivo: Measurements. *Spine*, **28** (2003) 2585. https://doi.org/10.1097/01.BRS.0000096673.16363.C7.
29. K. Chastain, B. Gepner, D. Moreau, B. Koerber, J. Forman, J. Hallman, & J. Kerrigan, Effect of axial compression on stiffness and deformation of human lumbar spine in flexion-extension. *Traffic Injury Prevention*, **24** (2023) S55–S61. https://doi.org/10.1080/15389588.2023.2198627.
30. K. Chastain, M. R. Burns, B. Gepner, J. Forman, J. Hallman, & J. Kerrigan, Effect of Axial Compression on the Kinetic and Kinematic Responses of Adult Male Human Lumbar Spine in Lateral Bending. (2023).
31. G. Wu, S. Siegler, P. Allard, C. Kirtley, A. Leardini, D. Rosenbaum, M. Whittle, D. D. D'Lima, L. Cristofolini, H. Witte, O. Schmid, & I. Stokes, ISB recommendation on definitions of joint coordinate system of various joints for the reporting of human joint motion—part I: ankle, hip, and spine. *Journal of Biomechanics*, **35** (2002) 543–548. https://doi.org/10.1016/S0021-9290(01)00222-6.
32. M. R. Burns, A. J. Caldwell, J. Shin, S. H. Sochor, K. P. Kopp, G. Shaw, B. Gepner, & J. R. Kerrigan, Assessing the ability of pressure sensors inserted into intervertebral discs to detect compression, flexion, and combined flexion + compression loading. (2024).
33. S. K. Tushak, J. Paul Donlon, B. D. Gepner, A. Chebbi, B. Pipkorn, J. J. Hallman, J. L. Forman, & J. R. Kerrigan, Failure tolerance of the human lumbar spine in dynamic combined compression and flexion loading. *Journal of Biomechanics*, **135** (2022) 111051. https://doi.org/10.1016/j.jbiomech.2022.111051.

VIII. APPENDICES

Appendix A:

TABLE AI
SPECIMEN INFORMATION

Specimen	Sex	Age	Height (cm)	Weight (kg)	BMI
945	Female	43	154.9	59.0	24.6
992	Male	40	180.3	87.1	26.8
1007	Male	63	172.7	83.9	28.1
1008	Male	45	182.9	83.9	25.1
1040	Female	66	162.6	82.5	31.2
1041	Female	85	167.6	76.2	27.1
1042	Female	75	160.0	49.9	17.8

Appendix B:

992M

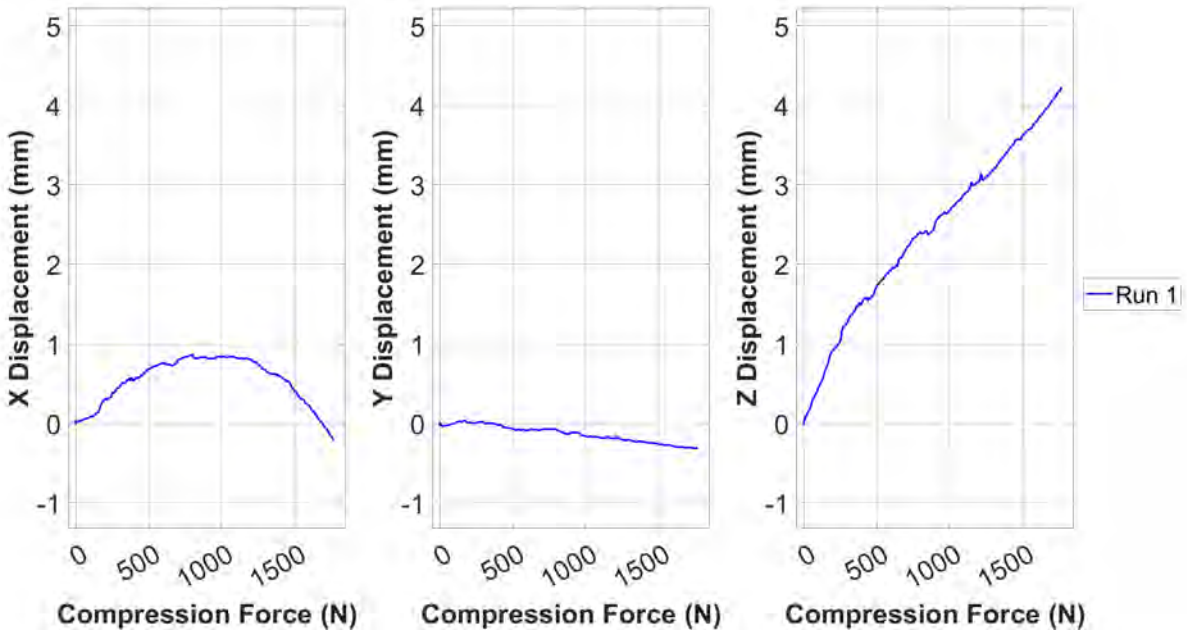

1007M

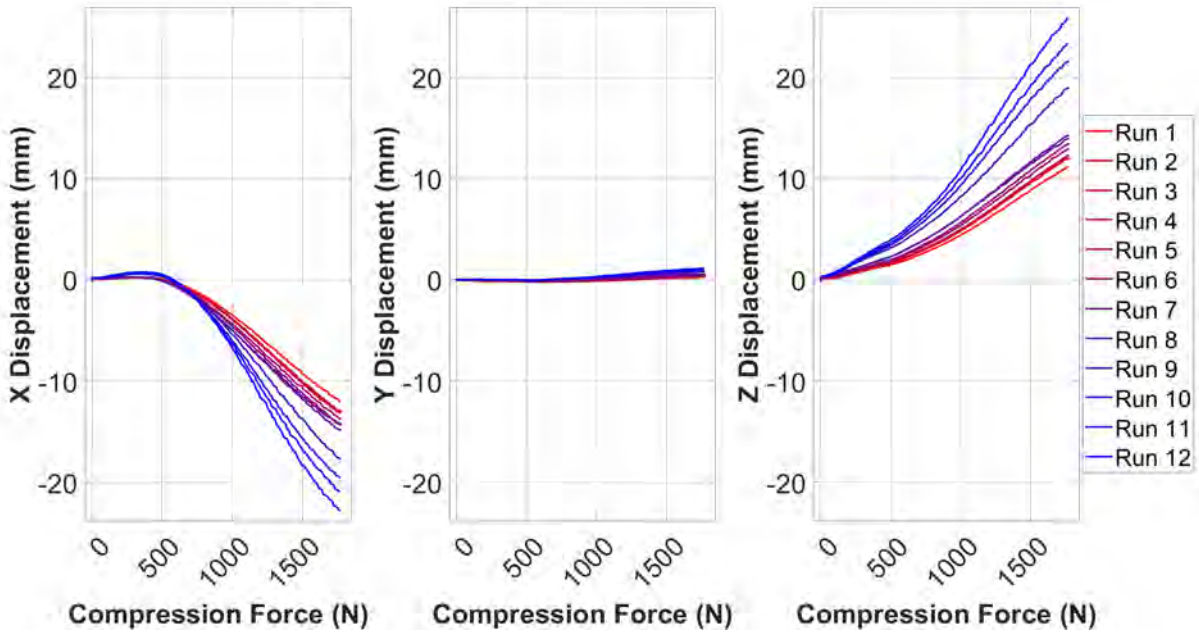

1008M

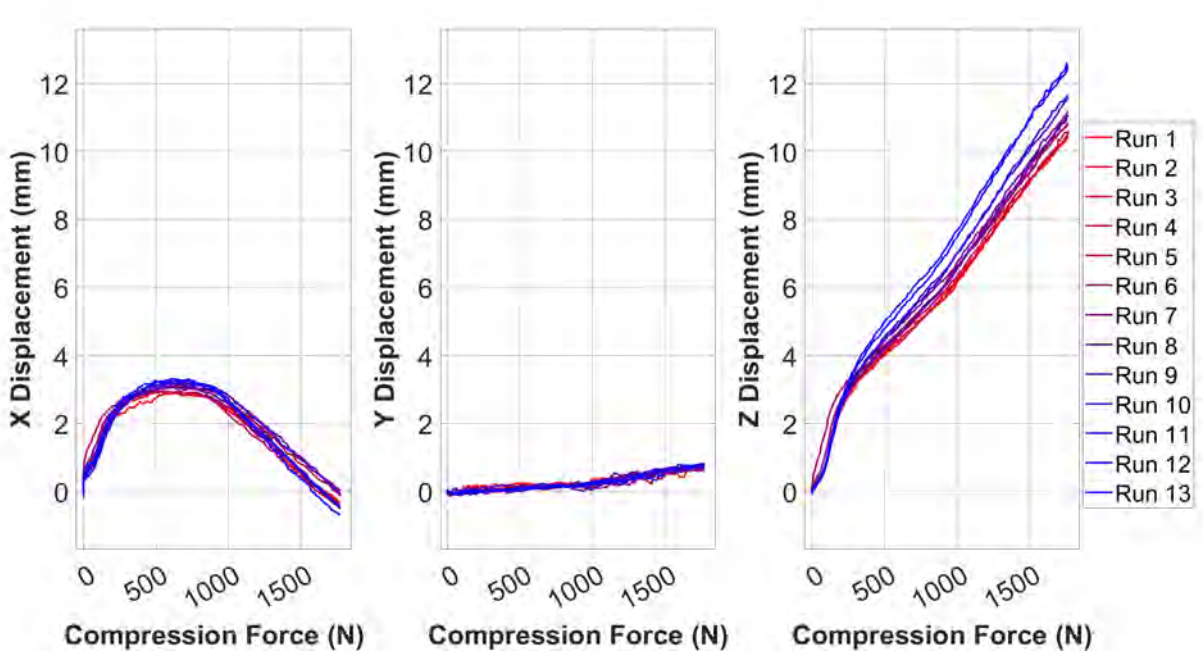
X Displacement (mm)
Y Displacement (mm)
Z Displacement (mm)
Compression Force (N)
Compression Force (N)
Compression Force (N)
Run 1
Run 2
Run 3
Run 4
Run 5
Run 6
Run 7
Run 8
Run 9
Run 10
Run 11
Run 12
Run 13

1040F

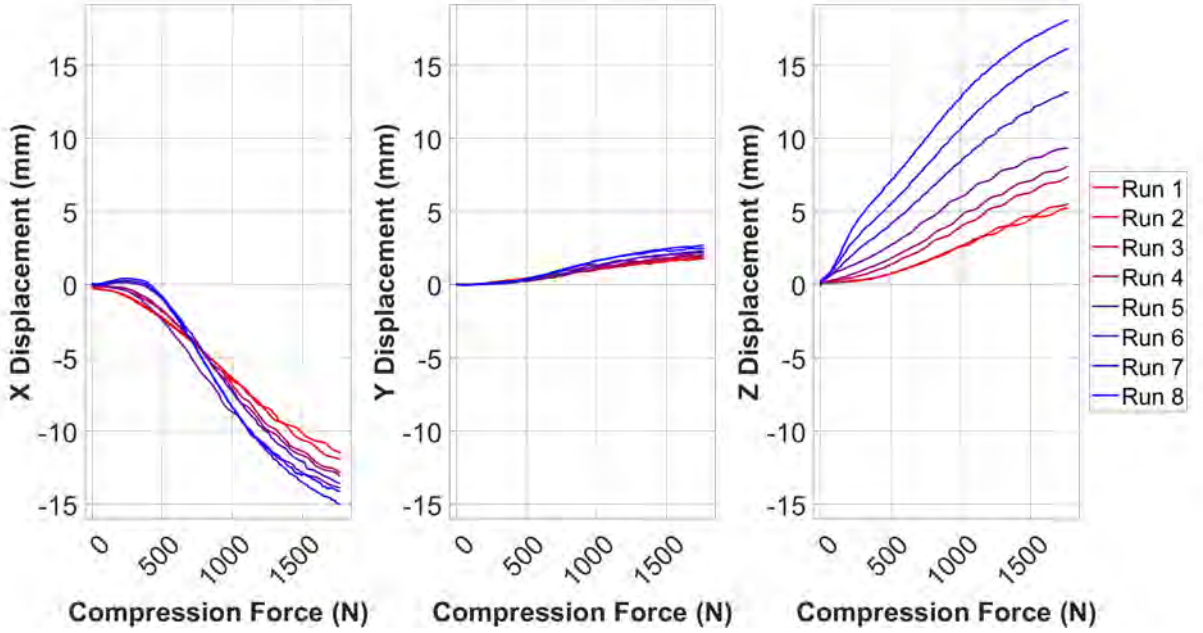
X Displacement (mm)
Y Displacement (mm)
Z Displacement (mm)
Compression Force (N)
Compression Force (N)
Compression Force (N)
Run 1
Run 2
Run 3
Run 4
Run 5
Run 6
Run 7
Run 8

1041F

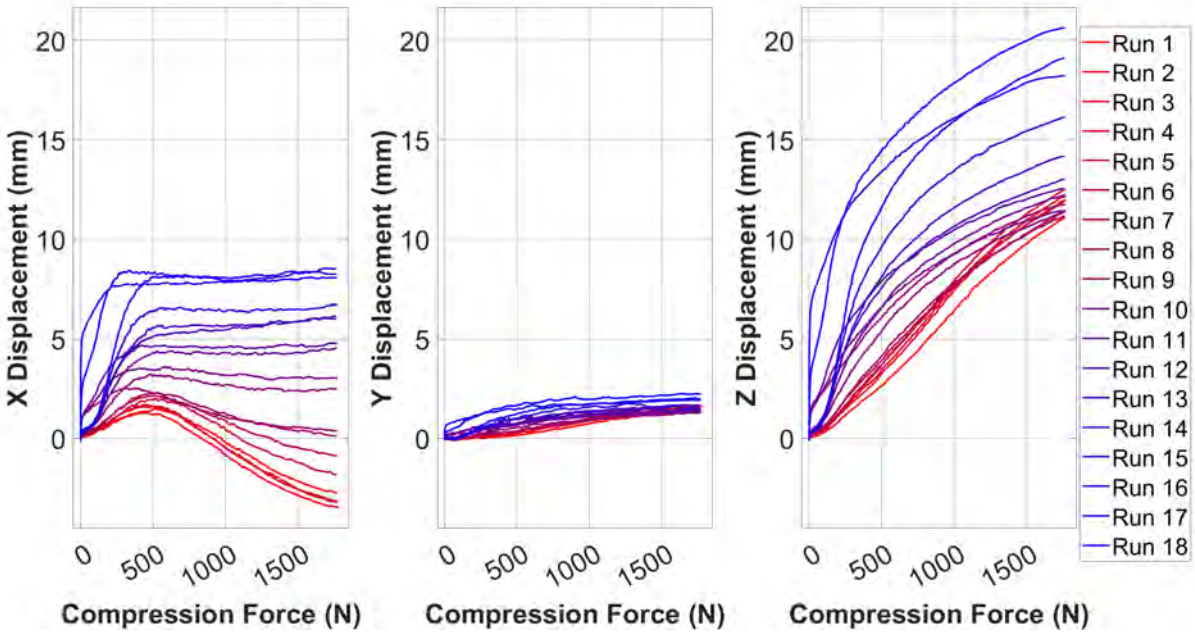

Fig. B1. Component displacements as a result of input compression force across trials for each specimen. Each trial is shown with its own line. Colours progress from red to blue with each test. Displacements in X are reported on the left, Y in the middle, Z on the right.

Appendix C:

992M

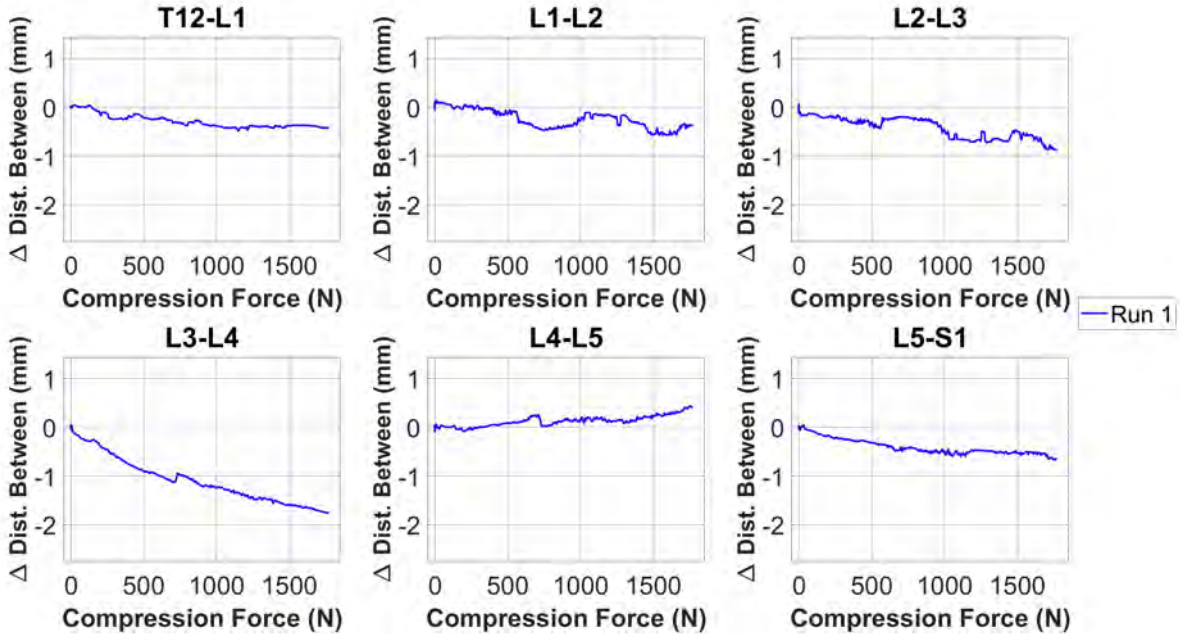

1007M

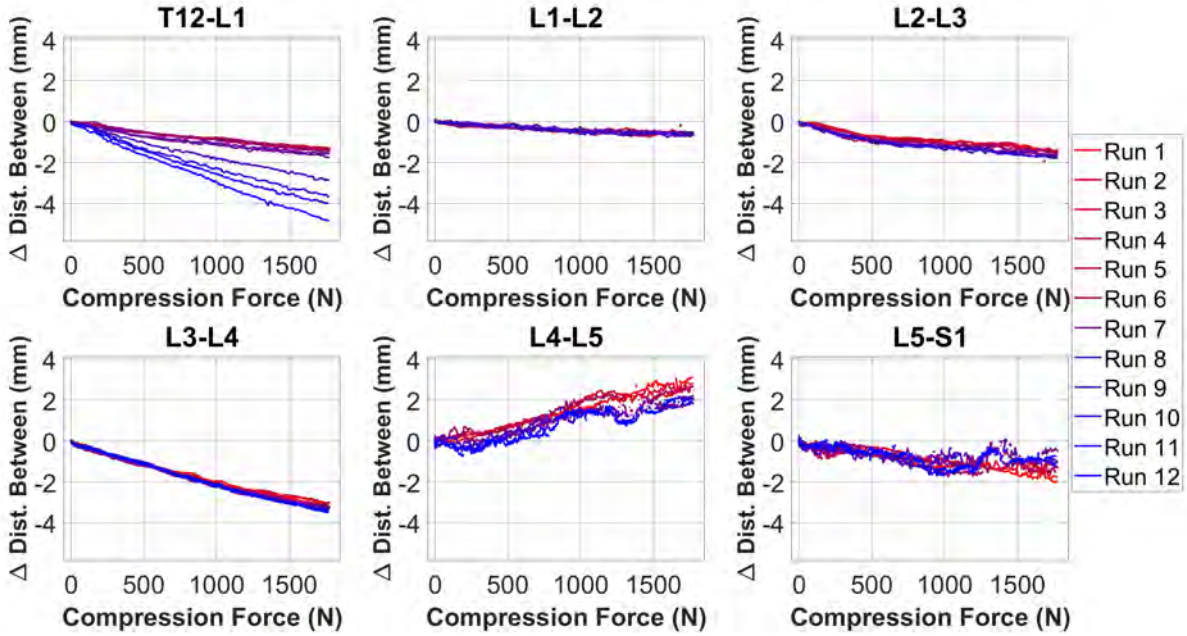

1008M

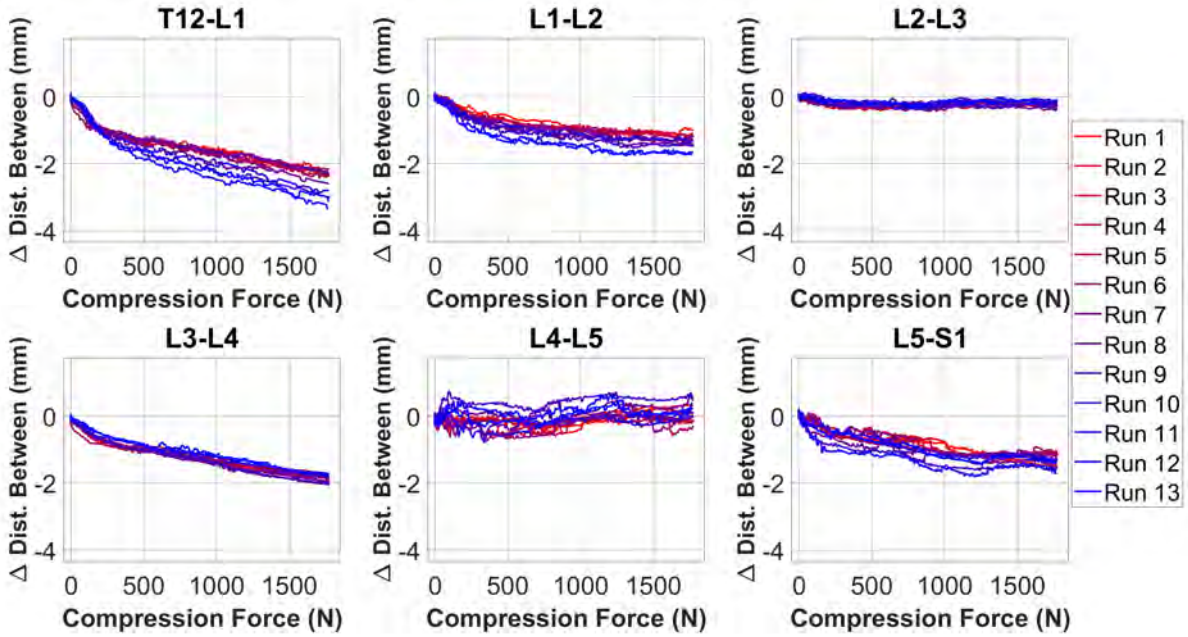
T12-L1
L1-L2
L2-L3
L3-L4
L4-L5
L5-S1
Δ Dist. Between (mm)
Compression Force (N)
0
-2
-4
0
500
1000
1500
Run 1
Run 2
Run 3
Run 4
Run 5
Run 6
Run 7
Run 8
Run 9
Run 10
Run 11
Run 12
Run 13

1040F

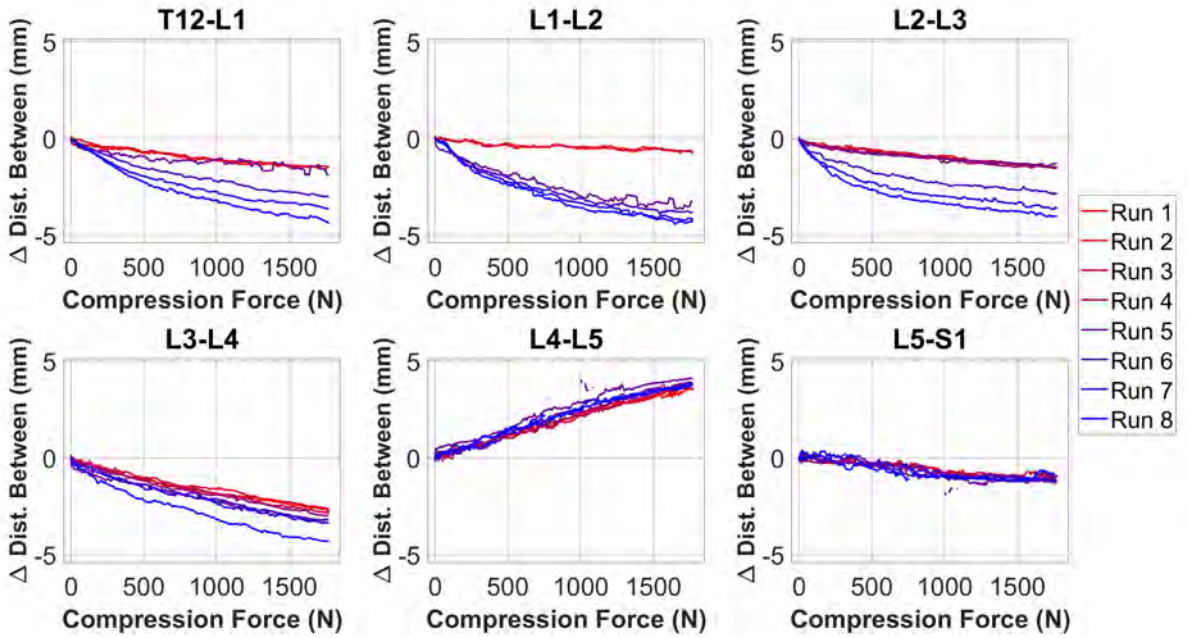
T12-L1
L1-L2
L2-L3
L3-L4
L4-L5
L5-S1
Δ Dist. Between (mm)
Compression Force (N)
5
0
-5
0
500
1000
1500
Run 1
Run 2
Run 3
Run 4
Run 5
Run 6
Run 7
Run 8

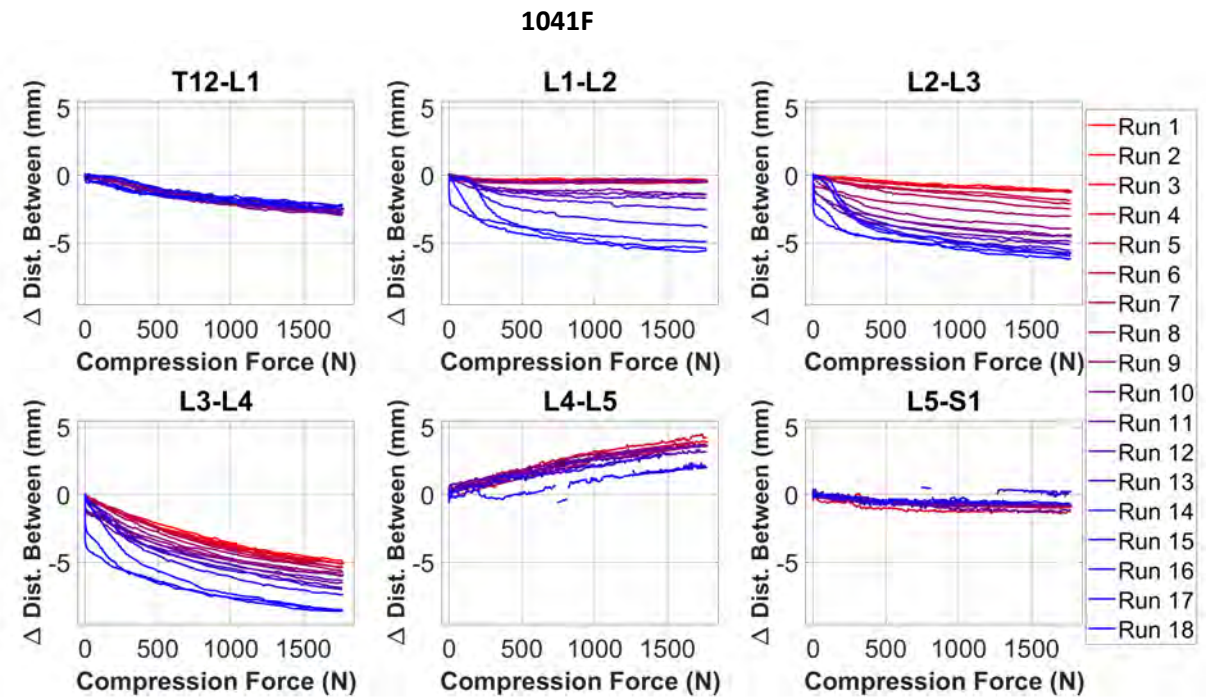

Fig. C1. Change in distance between neighbouring vertebral bodies with respect to input compression force across trials for each specimen. Each trial is shown with its own line. Colours progress from red to blue with each test. Change in distance between is reported for T12-L1 (top left), L1-L2 (top middle), L2-L3 (top right), L3-L4 (bottom left), L4-L5 (bottom middle), and L5-S1 (bottom right).

Appendix D:

945F

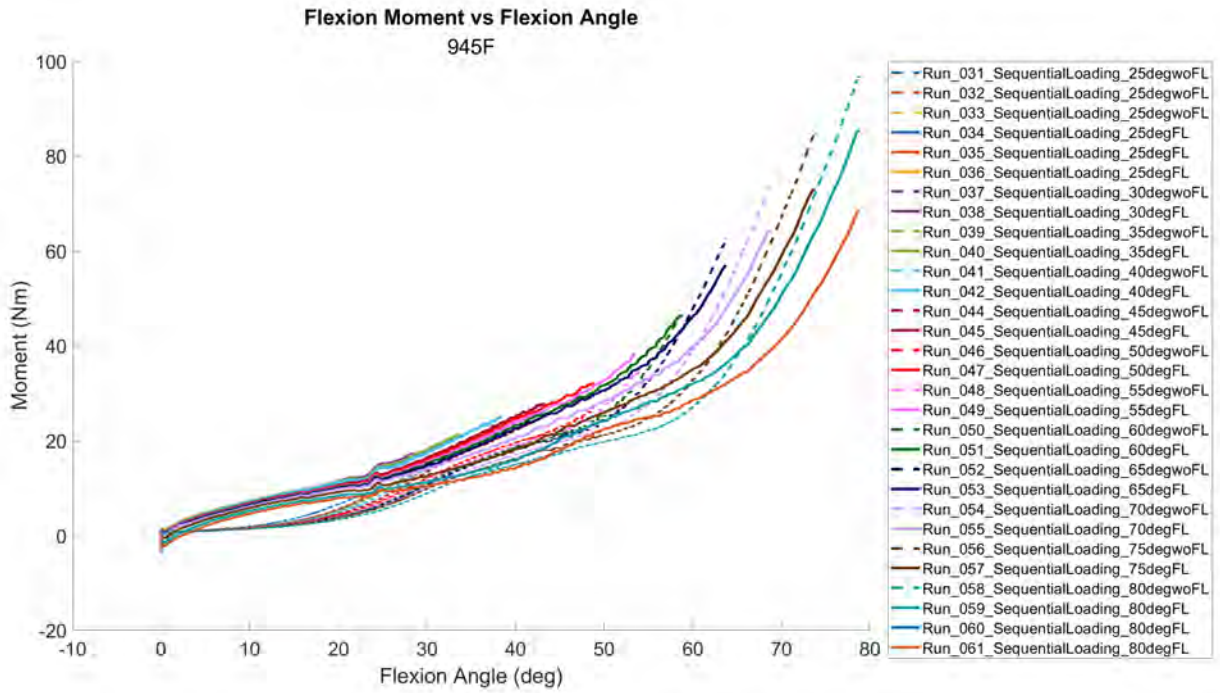

992M

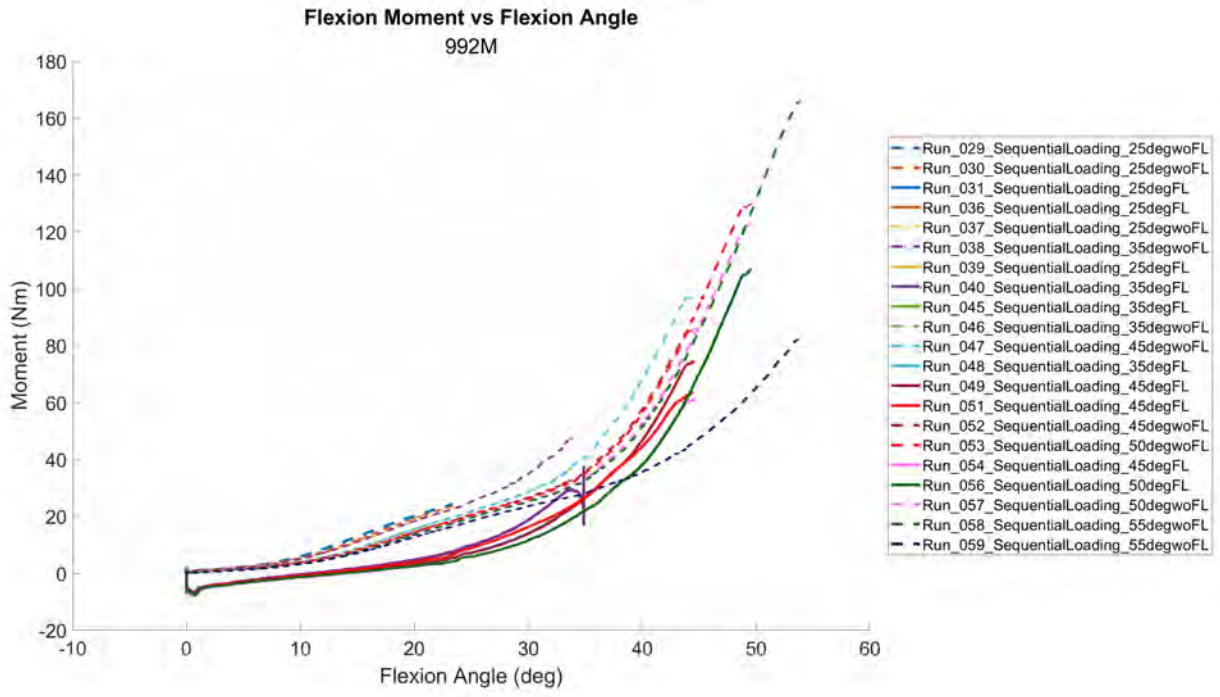

1007M

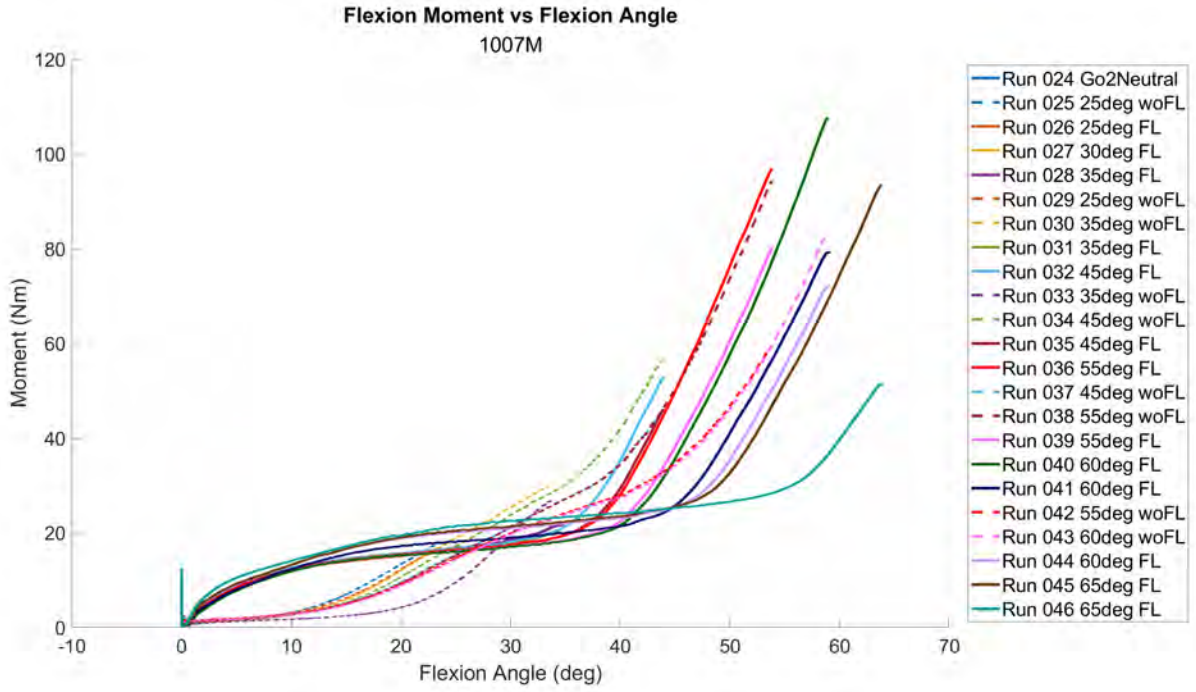
Flexion Moment vs Flexion Angle
1007M
Moment (Nm)
Flexion Angle (deg)
Run 024 Go2Neutral
Run 025 25deg woFL
Run 026 25deg FL
Run 027 30deg FL
Run 028 35deg FL
Run 029 25deg woFL
Run 030 35deg woFL
Run 031 35deg FL
Run 032 45deg FL
Run 033 35deg woFL
Run 034 45deg woFL
Run 035 45deg FL
Run 036 55deg FL
Run 037 45deg woFL
Run 038 55deg woFL
Run 039 55deg FL
Run 040 60deg FL
Run 041 60deg FL
Run 042 55deg woFL
Run 043 60deg woFL
Run 044 60deg FL
Run 045 65deg FL
Run 046 65deg FL

1008M

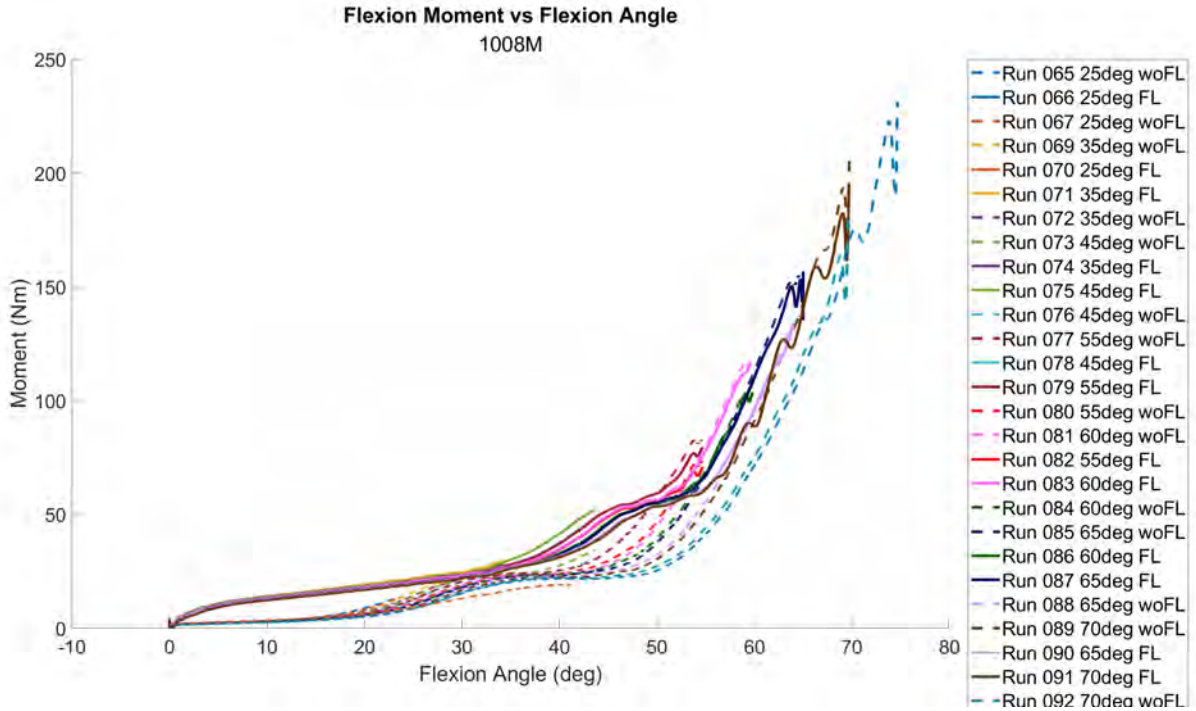
Flexion Moment vs Flexion Angle
1008M
Moment (Nm)
Flexion Angle (deg)
Run 065 25deg woFL
Run 066 25deg FL
Run 067 25deg woFL
Run 069 35deg woFL
Run 070 25deg FL
Run 071 35deg FL
Run 072 35deg woFL
Run 073 45deg woFL
Run 074 35deg FL
Run 075 45deg FL
Run 076 45deg woFL
Run 077 55deg woFL
Run 078 45deg FL
Run 079 55deg FL
Run 080 55deg woFL
Run 081 60deg woFL
Run 082 55deg FL
Run 083 60deg FL
Run 084 60deg woFL
Run 085 65deg woFL
Run 086 60deg FL
Run 087 65deg FL
Run 088 65deg woFL
Run 089 70deg woFL
Run 090 65deg FL
Run 091 70deg FL
Run 092 70deg woFL

1040F

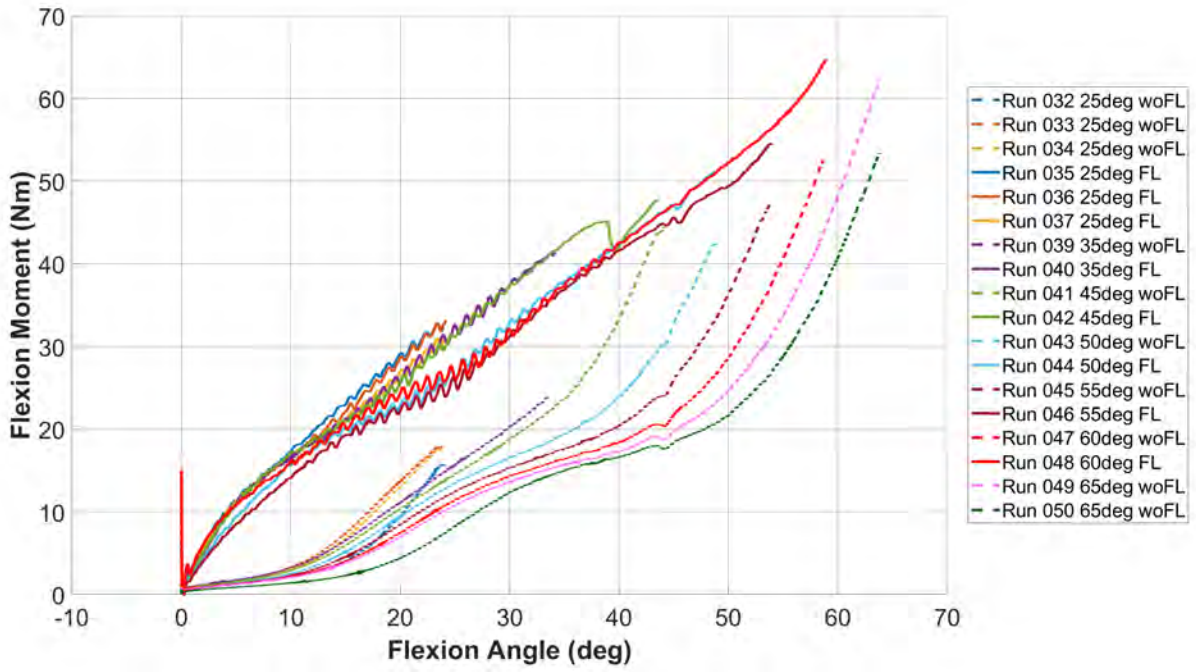

1041F

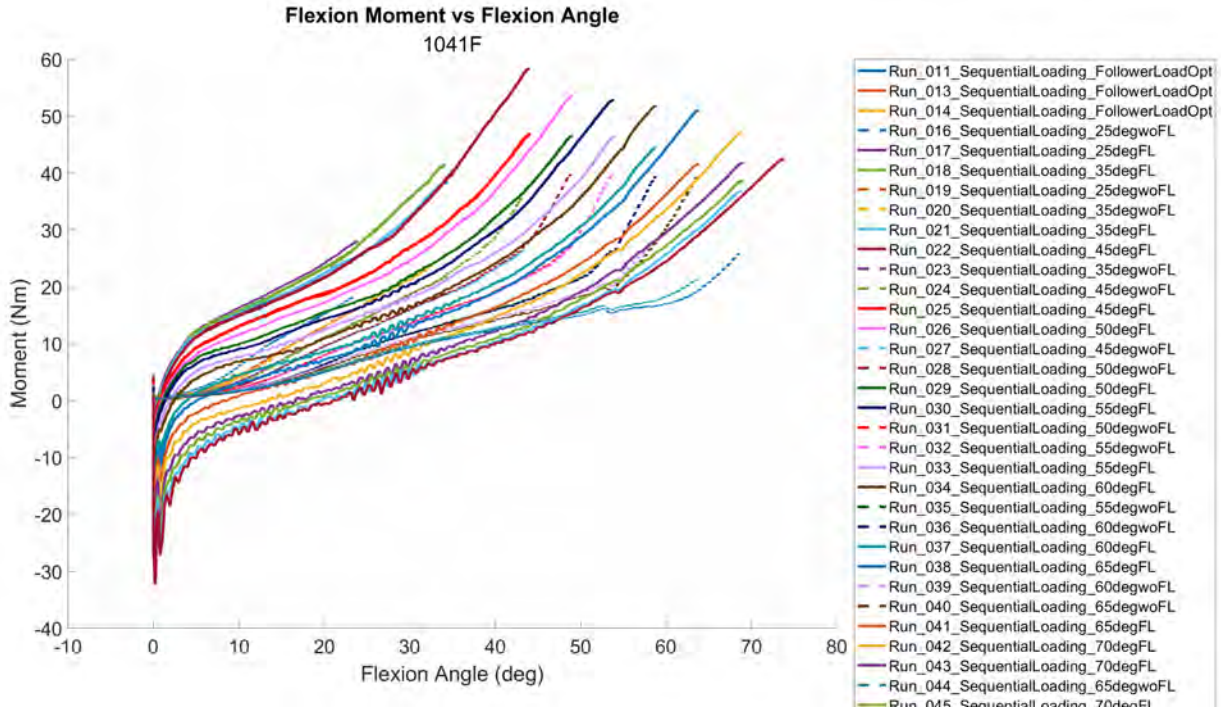

Fig. D1. Flexion moment versus flexion angle for all tests for a single specimen. Tests with and without follower load applied axial compression are included here. Each test of the sequential loading matrix is shown as its own line. Dashed lines represent the tests without axial compression, while solid lines represent the tests with axial compression.

Appendix E:

25 degrees without Axial Compression

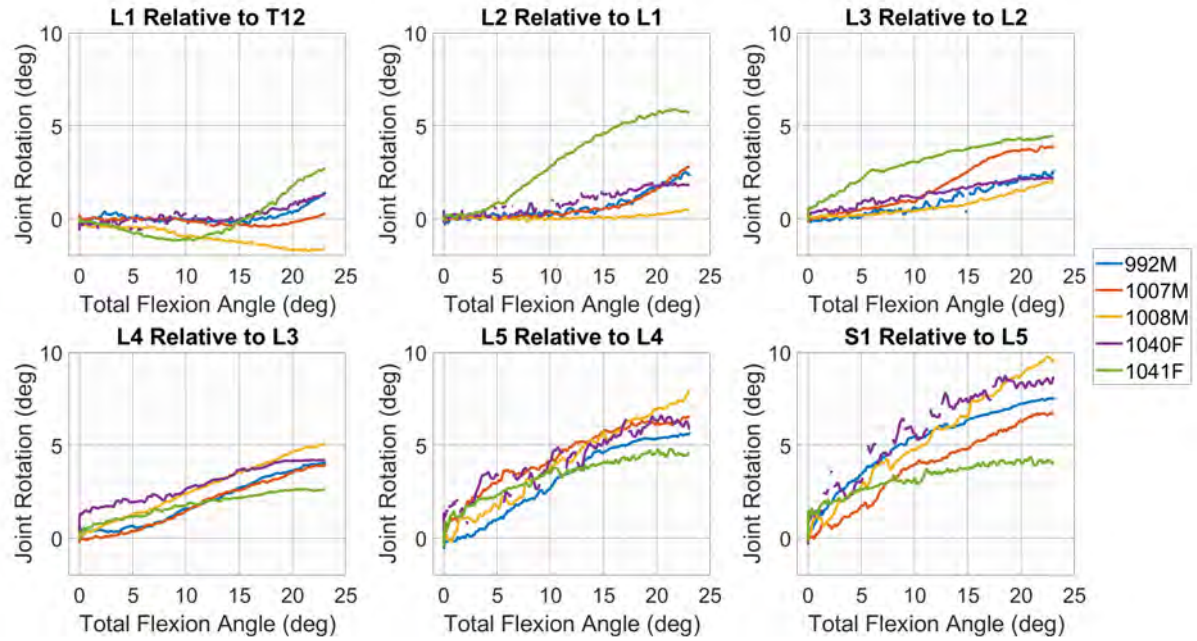

25 degrees with Axial Compression

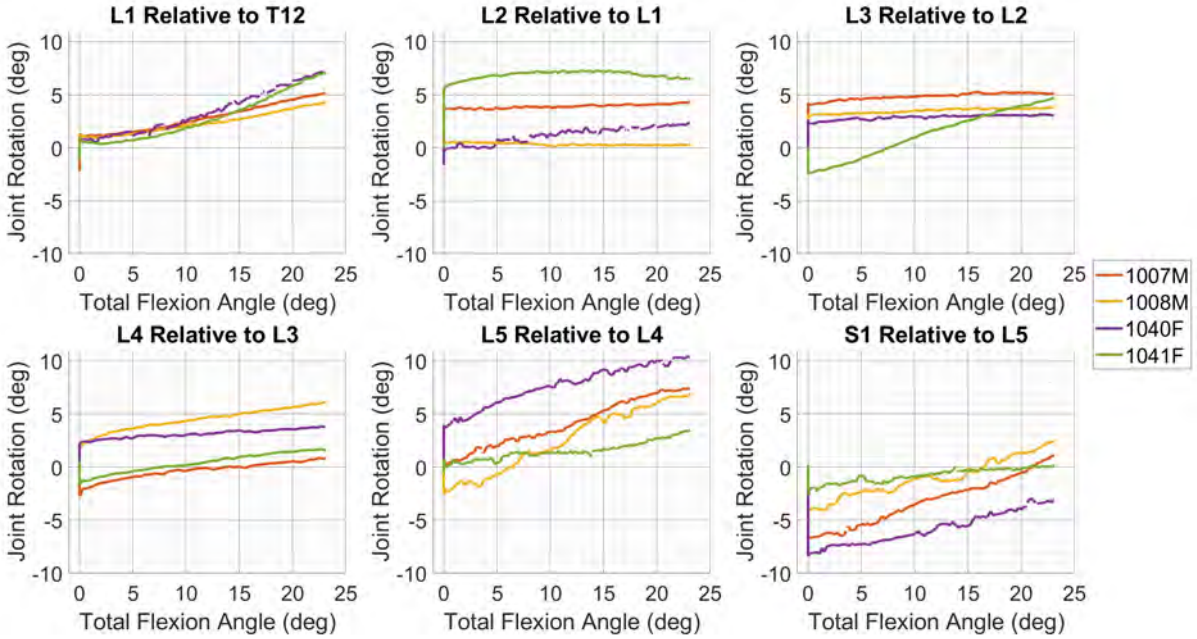

35 degrees without Axial Compression

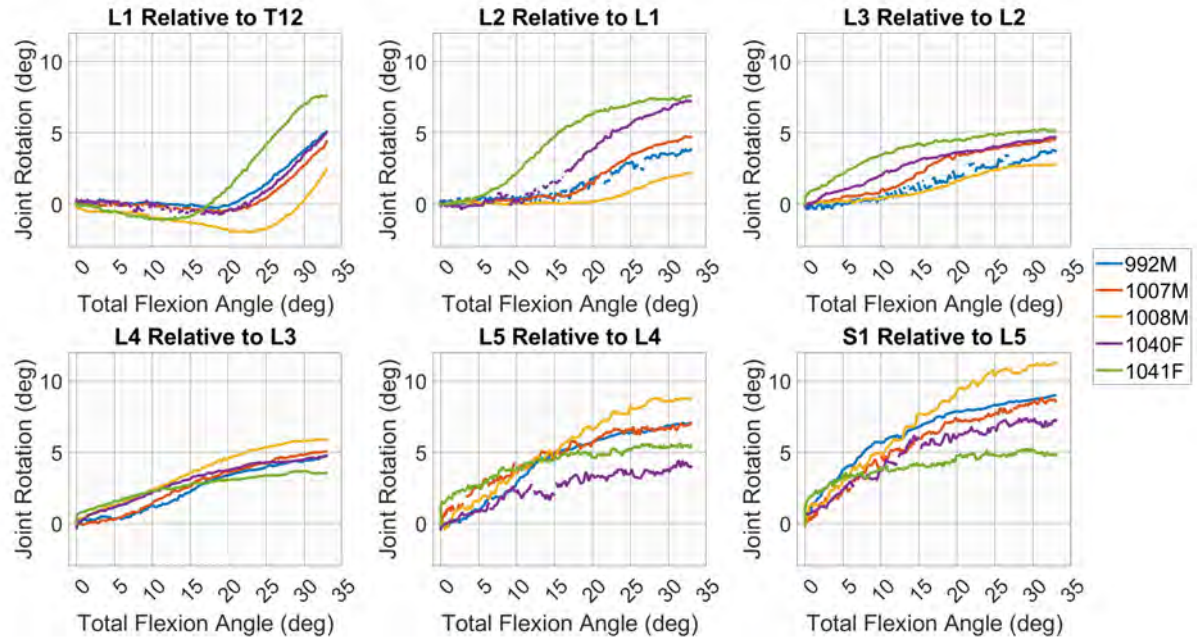

35 degrees with Axial Compression

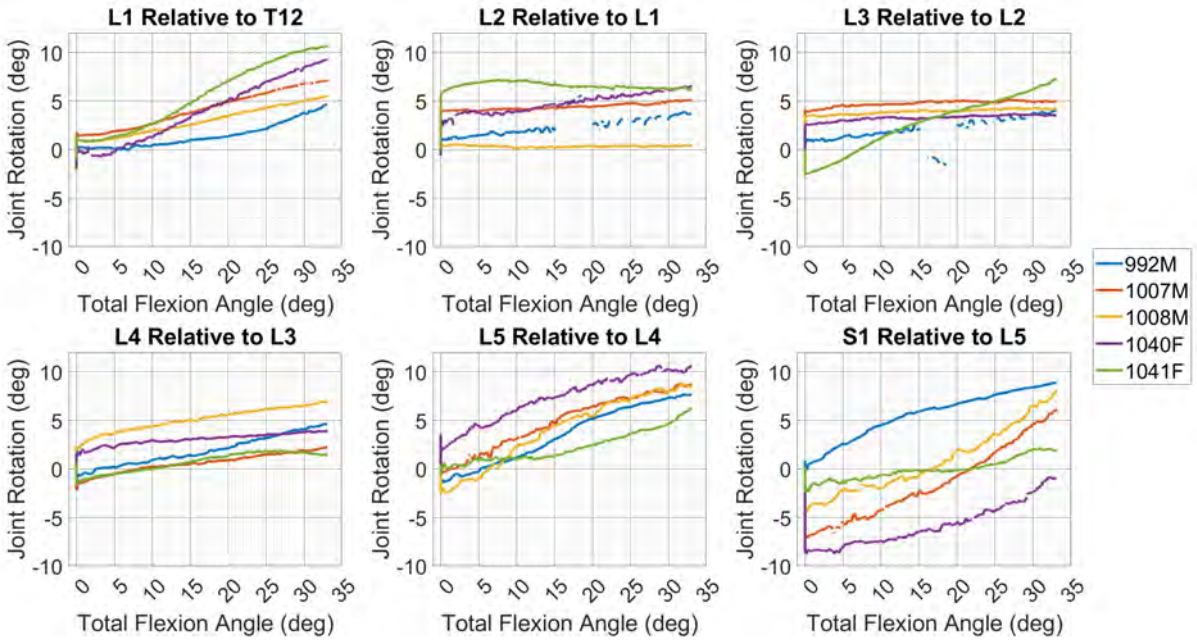

45 degrees without Axial Compression

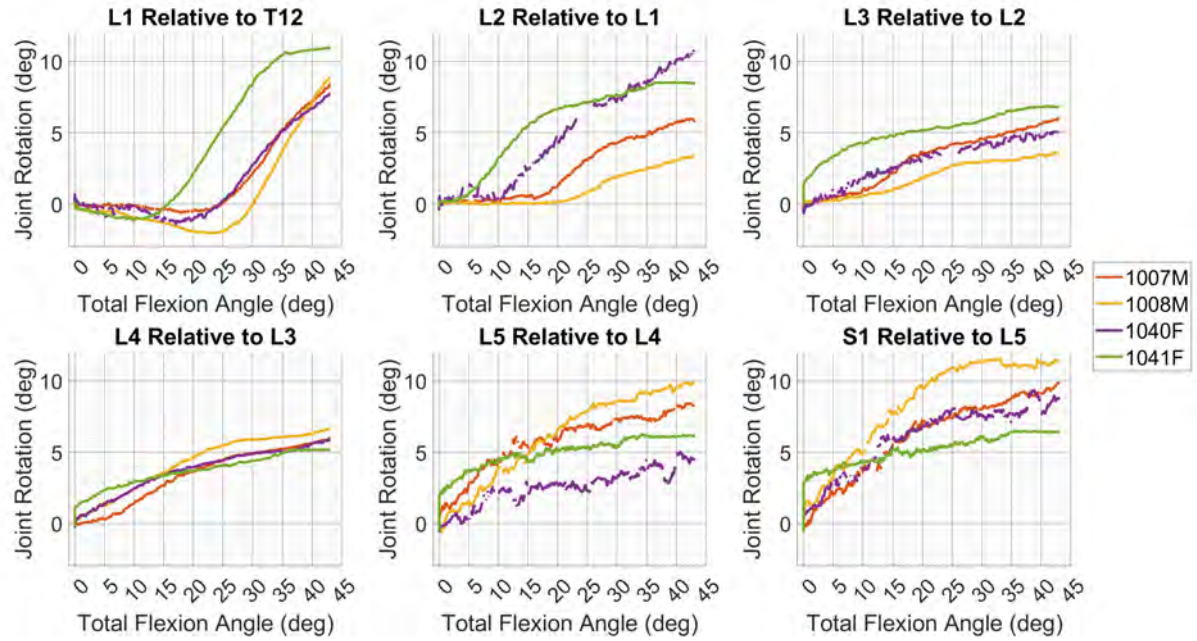

45 degrees with Axial Compression

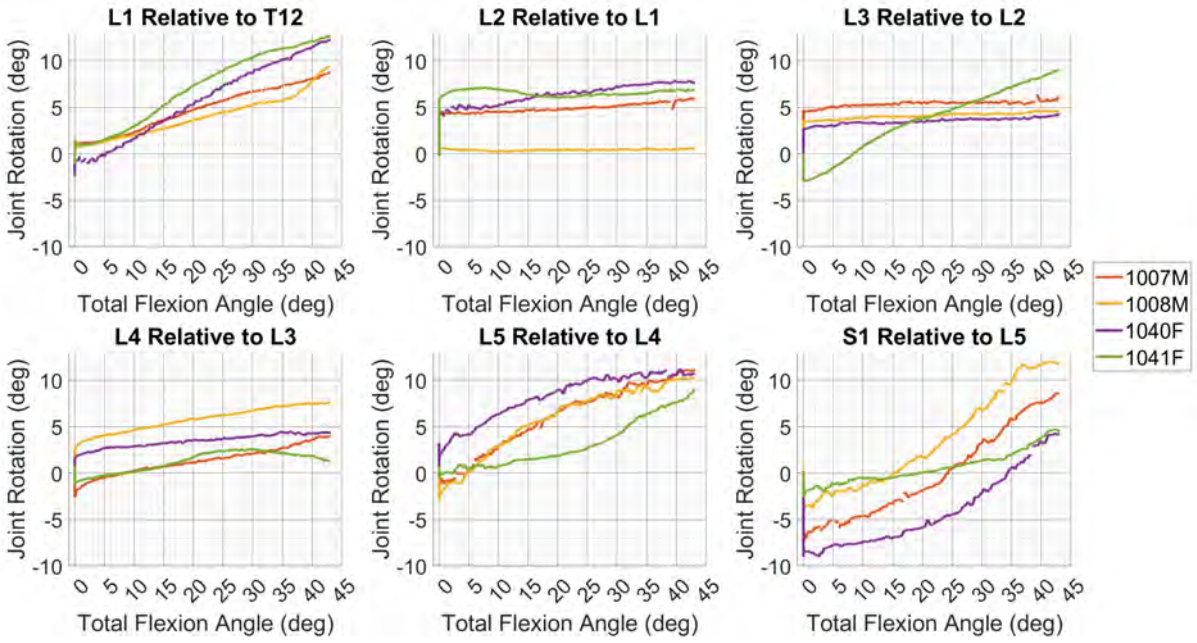

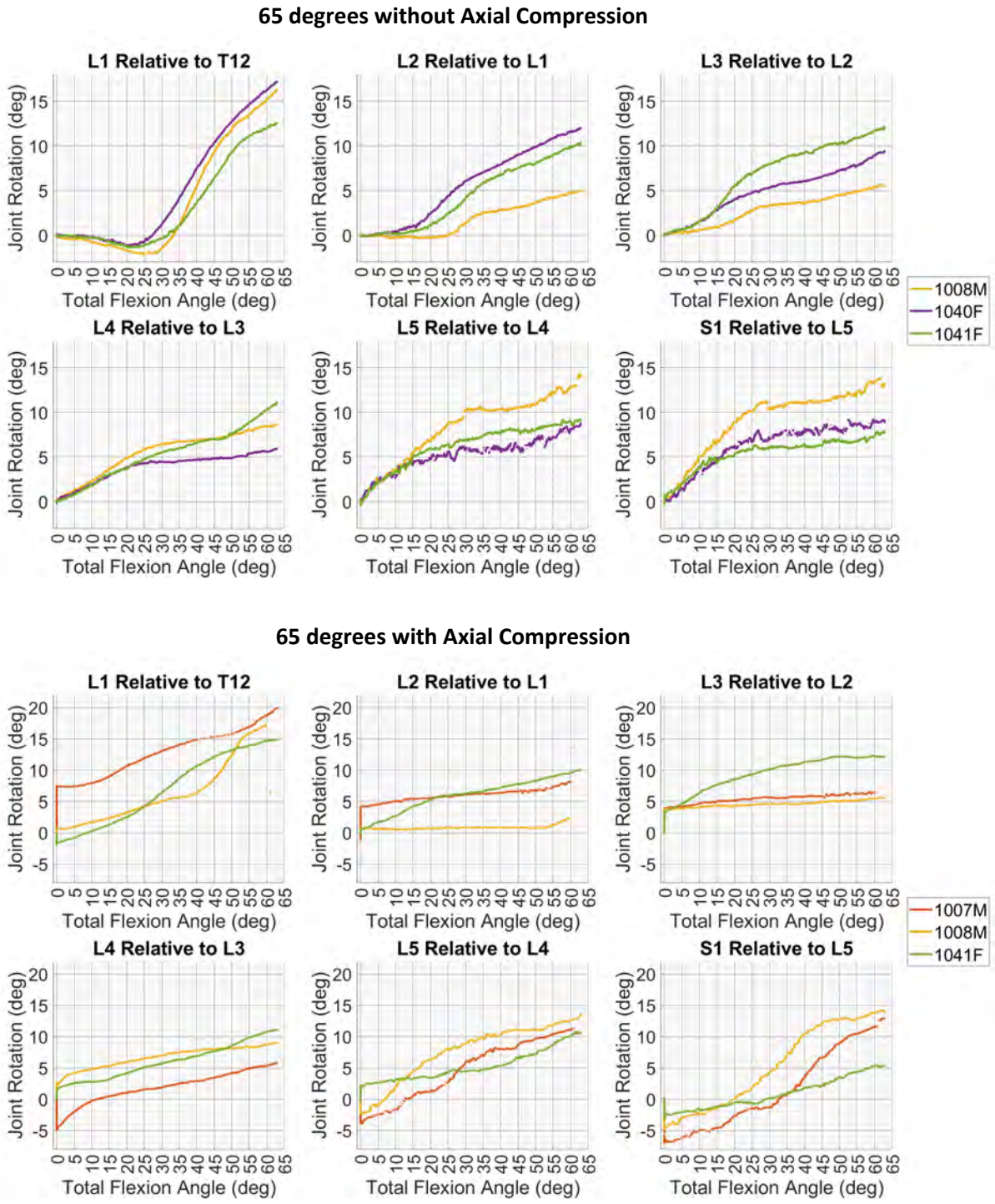

Fig. E1. Individual joint rotation for each of the six free joints versus the total spine flexion angle across specimens for each loading condition. Each line represents a different specimen. The first test in each loading condition is plotted, and no repeated tests are included.